



Numerical Heat Transfer, Part A: Applications

An International Journal of Computation and Methodology

ISSN: (Print) (Online) Journal homepage: www.tandfonline.com/journals/unht20

Bio-convection of ternary magnetized nanoparticles thermal conductivity in chemical reaction and activation energy flow with Darcy Forchheimer permeable across a double porous medium

Qadeer Raza, Xiaodong Wang, Hussein A. H. Muhammed, M. Zubair Akbar Qureshi, Ali J. Chamkha & Hassan Ali Ghazwani

To cite this article: Qadeer Raza, Xiaodong Wang, Hussein A. H. Muhammed, M. Zubair Akbar Qureshi, Ali J. Chamkha & Hassan Ali Ghazwani (16 Feb 2024): Bio-convection of ternary magnetized nanoparticles thermal conductivity in chemical reaction and activation energy flow with Darcy Forchheimer permeable across a double porous medium, Numerical Heat Transfer, Part A: Applications, DOI: [10.1080/10407782.2024.2316210](https://doi.org/10.1080/10407782.2024.2316210)

To link to this article: <https://doi.org/10.1080/10407782.2024.2316210>



Published online: 16 Feb 2024.



Submit your article to this journal [↗](#)





View related articles [↗](#)



View Crossmark data [↗](#)



Bio-convection of ternary magnetized nanoparticles thermal conductivity in chemical reaction and activation energy flow with Darcy Forchheimer permeable across a double porous medium

Qadeer Raza^a , Xiaodong Wang^a, Hussein A. H. Muhammed^a,
M. Zubair Akbar Qureshi^b, Ali J. Chamkha^c , and Hassan Ali Ghazwani^d

^aSchool of Mathematics and Statistics, Xian Key Laboratory of Scientific Computation and Applied Statistics, Northwestern Polytechnical University, Xi'an, P.R. China; ^bDepartment of Mathematics, Air University, Islamabad, Multan, Pakistan; ^cFaculty of Engineering, Kuwait College of Science and Technology, Kuwait City, Kuwait; ^dDepartment of Mechanical Engineering, College of Engineering, Jazan University, Saudia Arabia

ABSTRACT

This research focuses on investigating the impact of magnetized nanoparticles' heat and mass transfer process two-dimensional (2D) porous medium ternary hybrid Magnetohydrodynamics (MHD) ferrofluid flow through a two movable permeable porous surface, with a specific emphasis on the Darcy Forchheimer effect, activation energy, and chemical reaction parameters. Recently, motile microorganisms have become a significant area of interest in the study of heat and mass transfer. This study employs colored plots to analyze the optimum heat transfer over a double porous plate by altering different physical parameters. Using the shooting technique, the study provides numerical solutions to nonlinear systems of equations by transforming the partial differential equations (PDE) into ordinary differential equations (ODEs) via the dimensionless similarity transformation. Tables and graphs demonstrate how the governing parameters impact velocity, temperature, mass concentration profiles, and motile microorganisms, as well as physical quantities like skin friction coefficient, Nusselt number, Sherwood number, and motile number. Ternary hybrid ferrofluid exhibits a significantly improved heat transfer rate compared to both Ferro and hybrid ferrofluid. The convective flux of heat and mass transfer experiences a decrement with an escalation in the values of the activation energy (E) parameter. The presence of positive values for both the similarity variable (η) and Exothermic/Endothermic parameter (λ) leads to an enhancement in the flow of thermal transfer on both porous surfaces. This research will have far-reaching implications in various fields, including coolant technology in the manufacturing industry, heat dissipation in electronic modules, high-performance computing cooling facilities, the automotive sector, and space applications.

ARTICLE HISTORY


Received 8 November 2023
Revised 27 December 2023
Accepted 4 February 2024

KEYWORDS

And activation energy; chemical reaction; Darcy Forchheimer; heat and mass transfer of microorganisms; porous medium; ternary hybrid ferrofluid

1. Introduction

Motile microorganisms are single-celled organisms that are capable of movement. They can move spontaneously under various stimuli such as density, light, food, chemicals, oxygen, and gravitation. Motile microorganisms play an important role in many biological processes, including

CONTACT Qadeer Raza  qadeerraza@mail.nwpu.edu.cn  School of Mathematics and Statistics, Xian Key Laboratory of Scientific Computation and Applied Statistics, Northwestern Polytechnical University, Xi'an 710129, P.R. China; Hassan Ali Ghazwani  Hghazwani@jazanu.edu.sa  Department of Mechanical Engineering, College of Engineering, Jazan University, Jazan, Saudia Arabia.

Nomenclatures

F_{fd}	Ferrofluid	$(C_p)_{trihffd}$	Specific Heat of Ternary Hybrid Ferrofluid
HF_{fd}	Hybrid ferrofluid	$k_{trihffd}$	Thermal conductivity of Ternary Hybrid ferrofluid
$Trihffd$	Ternary Hybrid ferrofluid	N	Size of particles
k_{bf}	Shape factor for thermal conductivity base fluid	u, v	Velocity components
μ_{bf}	Dynamic viscosity of the base fluid	$\rho_{s1}, \rho_{s2}, \rho_{s3}$	Densities of Ferro particles 1, 2, and 3
ρ_{bf}	Water density (base fluid)	k_{s1}, k_{s2}, k_{s3}	Thermal conductivities for 1 st 2 nd and 3 rd nanoparticles
μ_{bf}	Water dynamic viscosity	η	Independent similarity variable
x, y	Coordinate axis	$\varphi_1, \varphi_2, \varphi_3$	Ferro particle's 1 st , 2 nd , 3 rd volume fraction
ν	Kinematic viscosity		
μ	Dynamic viscosity		
ρ	Density		
ρc_p	Specific heat capacity		
T	Temperature		

nutrient cycling, decomposition, and disease. They have also been studied extensively in the field of microfluidics, where they can be used to enhance mass transfer and microscale mixing in various nanofluids. Many studies have investigated bioconvection phenomena. For example, Algehyne *et al.* [1] investigated the flow of nanofluid with motile microorganisms over a vertical permeable surface with thermal slip conditions. Maatoug *et al.* [2] investigated the bioconvective Homann flow of tangential hyperbolic nanofluid across a revolving plate with convection and minimum mass flux limitations. With an emphasis on the consequences of the chemical reaction and heat production, Ahmad *et al.* [3] examined the mass as well as heat flow of gyrotactic microorganisms and nanomaterials across a porous medium. Puneeth *et al.* [4] explored the influence of gyrotactic microorganism movement on the heat and mass transfer properties of Casson nanofluid. Madkhali *et al.* [5] examined the impact of nanoparticles on flow behavior in the presence of motile microorganisms. Elayarani *et al.* [6] investigated the effects of gyrotactic microorganisms on heat and mass transfer in Magnetohydrodynamics (MHD) Carreau nanofluid flow, while Nisar *et al.* [7] analyzed the effects of motile gyrotactic microorganisms in the bioconvection peristaltic flow of Carreau-Yasuda bionanomaterials. Al-Bossly *et al.* [8] studied the flow of a stratified MHD Eyring-Powell fluid containing gyrotactic microorganisms through a stretching sheet with mixed convection. Sravanthi *et al.* [9] analyzed the impact of magnetic field and activation energy on nanofluid flow containing gyrotactic microorganisms on a stretching surface, while Pourrajab *et al.* [10] analyzed the bioconvection of nanofluid past a stretching sheet in a porous medium with gyrotactic microorganisms and Newtonian heating. Ahmad *et al.* [11] presented a numerical study of nanofluid flow containing gyrotactic microorganisms through a porous medium using the finite element method. Mondal *et al.* [12] studied the computational methods of the bioconvective stream of nanofluid containing gyrotactic microorganisms across a sheet of nonlinear stretching using the homotopy analysis approach.

Ferrofluid is a type of liquid that consists of small magnetic particles suspended in a carrier fluid, such as water or oil. Due to the magnetic properties of the particles, ferrofluids can be controlled by an external magnetic field, which makes them useful for various applications, such as in speakers and medical devices. A hybrid ferrofluid is a type of ferrofluid that contains both magnetic and non-magnetic particles, resulting in unique properties and behavior compared to traditional ferrofluids. They are of great interest in various fields, including biomedicine, energy, and materials science. A ternary hybrid ferrofluid refers to a type of magnetic fluid that consists of three components, typically a magnetic solid, a nonmagnetic liquid, and a surfactant. These types of fluids have unique properties that make them useful in a variety of applications, including heat and mass transfer. When a ternary hybrid ferrofluid is exposed to a magnetic field,

it forms a pattern of convection cells. By using a ternary hybrid ferrofluid, it is possible to create a more efficient system that can transfer heat and mass more effectively than traditional methods. Overall, the use of ternary hybrid ferrofluids in heat and mass transfer applications is an exciting area of research that has the potential to revolutionize the way we think about energy conversion and industrial processes. Khashi'Ve *et al.* [13] determined the flow of hybrid ferrofluid 3D over a permeable shrinking sheet under the impact of thermal production, momentum, and thermophoresis. The flow of a hybrid ferrofluid across a stretched surface at a stagnation point in the presence of a magnetic field and ferrofluid flow was studied by Rosli *et al.* [14]. The analysis is relevant for biomedical applications, such as drug delivery using magnetic nanoparticles. Anantha *et al.* [15] examined the effects of an erratic heat source and sink on the movement of a hybrid ferrofluid's radiative thin film. The findings have implications for the design and optimization of heat transfer systems in engineering applications. Zainodin *et al.* [16] studied the movement of a hybrid ferrofluid across a progressive flexibility training medium with thermal radiation and velocity slips under the impact of a varied magnetic parameter field. The flow and heat transfer properties of the ferrofluid are significantly influenced by the magnetic field and slip parameter, according to the results. The shifting Legendre collocation approach was proposed by Saranya *et al.* [17] for addressing the unsteady viscous-Ohmic dissipative hybrid ferrofluid flow across a cylinder. The results show that the method provides accurate solutions for the hybrid ferrofluid flow, and can effectively capture the effects of the magnetic field, viscous dissipation, and Ohmic heating. Hosseinzadeh *et al.* [18] explored the flow of micropolar hybrid ferrofluid across a vertical plate while taking into account different base fluids and nanoparticle form parameters. The study used numerical methods to investigate the impact of various factors on flow and energy transfer. Bilal *et al.* [19] studied the unsteady flow of a ternary hybrid nanofluid between two parallel plates while taking electro-viscosity, chemical reaction, and activation energy into account. The study analyzes the fluid's behavior using numerical techniques and discovers that the presence of nanoparticles and chemical reactions dramatically modify the flow properties. For a ternary nanofluid that is flowing around a rotating disk, the effects of Hall currents to understand irradiation mechanism *via* Homotopy Analysis Method (HAM), and electromagnetic forces to analyze flow convergences are agreed in Shamshuddin *et al.* [20], and Shahzad *et al.* [21]. Entropy generation refers to the irreversible increase in disorder or randomness within the physical system due to frictional losses, and heat transfer. Hybrid nanofluid flow under various conditions such as thermal dissipation and MHD have been investigated to extrapolate the thermal and profiles of the flow and it is well established in Salawu *et al.* [22], and Patil *et al.* [23]. Shamshuddin *et al.* [24], studied the heat exchange of Williamson fluid flow's chemical interaction and thermophoretic diffusion outcomes around a Riga plate porous media with nonlinearity radiation flux. While, Islam *et al.* [25], analyzed the Sisko fluid modeling and numerical convective heat transport dismissal over a stretching aperture with radiation and thermal squandering. Ternary hybrid nanofluids, interfacial nanolayer and hybrid nanofluids flow under various magnetic forces, morphology, gyrotactic microorganisms while passing through a porous surface, in addition to the influences of chemical reaction, and activation energy is quite important to comprehensively understand the full picture of recent flow problems in fluids' flow [26–29].

Magnetohydrodynamics (MHD) has gained wide popularity in scientific and engineering applications in recent decades. Many studies have been carried out to examine the behavior of MHD under various situations. For instance, Tlili *et al.* [30] studied the influence of asymmetry temperature rapid rise on the MHD hybrid ferrofluid film flow to comprehend its behavior in MHD systems, which may have significant uses in cooling and heat transfer technologies. Anuar *et al.* [31] examined the flow of a hybrid ferrofluid over a permeable surface under the influence of a magnetic field and a heat source/sink in the stagnation point region. Zainodin *et al.* [16] analyzed the flow of heat and mass transfer effect of MHD mixed convection in a hybrid ferrofluid flow over a porous surface. Sandeep *et al.* [32] investigated the effects of radiation and magnetic field on the flow and

heat transfer behavior over a stretching sheet. Ferdows *et al.* [33] analyzed the effects of magnetic field and gyrotactic microorganisms on heat and mass transfer during nanofluid flow over a stretching/shrinking sheet. Hossain *et al.* [34] studied MHD heat and mass transfer flow in a high porosity medium and revolving system, taking into account Hall and ion-slip currents effects. Chamkha *et al.* [35] investigated the time-dependent flow of MHD heat and mass transfer in the forward stagnation region of a rotating sphere using mixed convection flow at different wall conditions. Rauf *et al.* [36] determined the impact of MHD flow of heat transfer in hybrid ferrofluid with nonlinearity and flow characteristics. Anantha *et al.* [15] studied the effect of irregular heat source/sink on the radiative thin film flow of MHD hybrid ferrofluid and provided a mathematical model to predict the fluid flow under the given conditions.

Darcy-Forchheimer is a mathematical model that describes fluid flow through porous media. It is an extension of Darcy's law that takes into account the effect of inertial forces on the flow, which is significant when the flow velocity is high. The model includes two terms: the Darcy term, which describes the flow due to pressure gradients, and the Forchheimer term, which accounts for the drag force due to the fluid's motion through the porous media. The Darcy-Forchheimer model is commonly used in the study of fluid flow in porous media, such as in the petroleum industry, groundwater hydrology, and filtration systems. The flow of nanofluid through porous media has been extensively studied due to its numerous applications in industrial and environmental systems. Taseer *et al.* [37] investigated the Darcy-Forchheimer flow of nanofluid through a porous non-Darcian medium, while Sheikholeslami *et al.* [38] investigated the flow of a non-Darcy Fe_3O_4 -water nanofluid in the influence of an external magnetic field across an unstable permeable medium. Saif *et al.* [39] analyzed the Darcy-Forchheimer flow of viscous nanofluid over a curved stretchable surface. Majeed *et al.* [40] investigated the Darcy-Forchheimer flow of an MHD viscous fluid across a linear extensible medium. Punith *et al.* [41] studied the flow of an incompressible dusty hybrid nanofluid across a stretched cylinder while taking the Darcy-Forchheimer porous medium and viscous dissipation into attention. Mallikarjuna *et al.* [42] designed a mathematical model of a two-phase dusty hybrid nanofluid flow over a stretching sheet with heat transfer in a porous medium, taking into account the Darcy-Forchheimer flow, viscous dissipation, and melting effect. Alshehri *et al.* [43] analyzed the flow of comparison on hybrid nanofluid and nanofluid impact of Darcy-Forchheimer across a slick nonlinear, non-uniform stretching surface. Nasir *et al.* [44] investigated the reactive MHD Darcy-Forchheimer fluid movement with radiation impact on a stretching exponential porous medium. The impact of temperature conduction and Brownian motion on combined convection heat and mass transport of nanofluid through a porous plate in a Darcy-Forchheimer flow were explored by Essam *et al.* [45]. Sindhu *et al.* [46] studied the Darcy-Forchheimer flow of a double-hybrid nanofluid approaching a Riga plate in the presence of radiation and heat source/sink influences. Upreti *et al.* [47] investigated the two different movable surfaces 3-D flow of heat transfer in the nanofluid Darcy-Forchheimer flow model. Mkhathshwa *et al.* [48] examined the electromagnetic flow of Carreau hybrid nanofluid in the direction of a stretch sheet in a Darcy-Forchheimer permeable material with the occurrence of slip boundary conditions.

Chemical reactions and activation energy refer to the study of chemical reactions that occur within a fluid or at the interface between two fluids. Activation energy is the energy required to initiate a chemical reaction. In fluid mechanics, activation energy is an important parameter that governs the rate at which reactions occur. Higher activation energies typically result in slower reaction rates, while lower activation energies result in faster reaction rates. Activation energy can be affected by various factors, such as temperature, pressure, and the presence of catalysts. This area of study is important for a variety of applications, including chemical processing, combustion, and environmental engineering. Overall, the study of chemical reactions and activation energy in fluid mechanics is essential for understanding and optimizing a wide range of industrial and environmental processes. According to Li *et al.* [49], magnetohydrodynamic flow

in a horizontal channel with revolving plates was investigated concerning the impacts of activation energy and chemical reaction. The effects of numerous conditions on fluid flow across porous materials are investigated in such research. Xiu *et al.* [50] investigated the joint influence of Lorentz force, component micro-rotation, and particle thermo-migration on the dynamics of micropolar fluids with nonlinear thermal radiation and Kinetics chemical reaction correlated to the activation energy. Khan *et al.* [51] looked at the temperature profile of a bioconvective flow of Maxwell nanoparticles in a porous media across an expanding and rotating cylinder, where the fluid flow reacts with chemically reactive activation energy. Hussain *et al.* [52] conducted a mathematical and analytical investigation to investigate the combined impact of activation energy and chemical reaction on the flow of nanofluids caused by a thin vibrating needle. Dessie *et al.* [53] explored the MHD flow of a Maxwell fluid in a moving frame and the way chemical reactions, activation energy, and thermal radiation impact it. Under activation energy, Hussain *et al.* [54], studied effects of thermal and stratifications-based of the polymeric nanofluids flow. Waqas *et al.* [55], inclusively investigated the role gyrotactic microorganisms, magnetohydrodynamics and stratifications on bioconvective Casson nanofluids. Tabrez and Khan [56], prospected the viscous dissipation leverages and magnetic-field polarity on an exotic ferromagnetic-polymeric-nanoliquid flow to gain insights on the physical system characteristics. Eyring Powell modified nanofluid flow has received considerable research efforts under various conditions and assumptions including activation energy, bioconvection dynamics, ferromagnetic effects and chemical reaction due to the gap discovered in literature as in Anjum *et al.* [57]. It can also be thoroughly found in Irfan *et al.* [58], some aspects of non-Fourier heat flux analysis for ferromagnetic Powell-Eyring fluid under chemical reaction conditions. The influence of bio-convection and thermal conduction on activation energy and chemical reaction kinetics in ternary magnetized nanofluid flows has become a major area of focus in recent years. However other research focused on and investigated magnetized various nanofluids flow models under many different physical conditions, coordinates and fluidic parameters [59–63]. Activities of gyrotactic microorganisms, nanoparticles on viscoelastic fluids, stratification phenomena, prominence of heat generation in chemically reactive, and melting heat transport characteristics effects on nanofluids' as to gain an enhanced hydromagnetic and stratification-based entropy fluids' flow have been an incredible research realm for in very recent years [64–69] to further understand the complex flow also, under dissipation aspect and Robin conditions.

The objective of this current research is to examine how the presence of Darcy-Forchheimer's double porous medium affects the flow characteristics of an incompressible, two-dimensional, laminar, ternary hybrid ferrofluid. This investigation encompasses the dynamics of heat and mass transfer in the context of motile microorganisms. In an extension of prior studies, we performed a numerical analysis to understand the behavior of the tri-hybrid ferrofluid during its flow. To facilitate this analysis, we applied the Shooting technique, a method that transforms the arrangement of partial differential equations (PDEs) into ordinary differential equations (ODEs). Solving these ODEs numerically allowed us to gain insights into the intricate behavior of the system. The outcomes of our study are presented through numerical and graphical representations, illustrating the contributions of various model factors. These factors include velocity, temperature, concentration, and motile profiles. Furthermore, our numerical analysis delved into examining key physical parameters associated with the flow over the porous surface. This investigation encompassed an exploration of skin friction coefficients, Nusselt number, Sherwood number, and the motile number.

2. Mathematical formulation

Porous medium 2 dimensional Darcy Forchheimer tri hybrid ferrofluid flow of heat and mass transfer with activation and chemical reaction are moving across two permeable plates. The classical liquid water in this work is viewed as a based liquid and three different magnetic nanoparticles.

The ternary hybrid ferrofluid is suspected to be incompressible and the flow is laminar. The porous channels, translate above the surface and below the surface with uniform velocity $c'(t)$ and are at a variable distance $2c(t)$. The geometry of the current issue exhibits the cartesian coordinates foundation, with the beginning point at the middle of the channel and absorbent walls that can allow fluid to influx or emit as the channel walls widen or contract. In addition, the y -axis is orthogonal to the channel walls. The induced magnetic field is ignored because of the low Reynolds number assumption. The fluid flow of the velocity field is used by $\mathbf{v} = (u(x, y, t), v(x, y, t))$. The flow is directed from left to right. Thermal equilibrium is considered to exist between the liquid (water) and the tri-hybrid ferrofluid. Figure 1 depicts the physical difficulty of the flow idea and coordinates. The concept expressions are, thus, presented as follows:

$$\frac{\partial u}{\partial x} + \frac{\partial v}{\partial y} = 0, \tag{1}$$

$$\frac{\partial u}{\partial t} + u \frac{\partial u}{\partial x} + v \frac{\partial u}{\partial y} = -\frac{p_x}{\rho_{hffd}} + \nu_{trihffd} \left(\frac{\partial^2 u}{\partial x^2} + \frac{\partial^2 u}{\partial y^2} \right) - \frac{\nu_{trihffd}}{k^*} (u) - \frac{1}{\rho_{trihffd}} F'(u^2) - \frac{\sigma_e B_0^2}{\rho_{trihffd}}, \tag{2}$$

$$\frac{\partial v}{\partial t} + u \frac{\partial v}{\partial x} + v \frac{\partial v}{\partial y} = -\frac{p_y}{\rho_{trihffd}} + \nu_{trihffd} \left(\frac{\partial^2 v}{\partial x^2} + \frac{\partial^2 v}{\partial y^2} \right), \tag{3}$$

$$\frac{\partial T}{\partial t} + u \frac{\partial T}{\partial x} + v \frac{\partial T}{\partial y} = \alpha_{trihffd} \left(\frac{\partial^2 T}{\partial x^2} + \frac{\partial^2 T}{\partial y^2} \right) + \frac{1}{(\rho_{cp})_{trihffd}} \left(\beta k_r^2 \left(\frac{T}{T_2} \right)^n * \exp \left(\frac{-E_a}{k^* T} \right) (C - C_2) \right), \tag{4}$$

$$\frac{\partial C}{\partial t} + u \frac{\partial C}{\partial x} + v \frac{\partial C}{\partial y} = (D_b)_{trihffd} \left(\frac{\partial^2 C}{\partial x^2} + \frac{\partial^2 C}{\partial y^2} \right) - k_r^2 \left(\frac{T}{T_2} \right)^n * \exp \left(\frac{-E_a}{k^* T} \right) (C - C_2), \tag{5}$$

$$\frac{\partial N}{\partial t} + u \frac{\partial N}{\partial x} + v \frac{\partial N}{\partial y} + \frac{bW_c}{C_1 - C_2} \frac{\partial}{\partial y} \left(N \frac{\partial C}{\partial y} \right) = (D_n)_{trihffd} \frac{\partial^2 N}{\partial y^2}. \tag{6}$$

Where $\rho_{trihffd}$, σ_e , B_0^2 , $\alpha_{trihffd}$, $(D_b)_{trihffd}$, $\nu_{trihffd}$, p , T , C , N , $(D_n)_{trihffd}$, $(D_n)_{trihffd}$, E_a , k^* , β , k_r^2 shows the density, electrical conductivity, strength of the magnetic field, thermal diffusivity, Diffusion coefficient of mass transfer, kinematics viscosity pressure, temperature, Concentration, motile microorganism, mass diffusion coefficient, bio convection diffusion coefficient, activation energy Boltzmann constant, Exothermic/endothermic co-efficient and Chemical reaction fixed parameter of a ternary Hybrid ferrofluid.

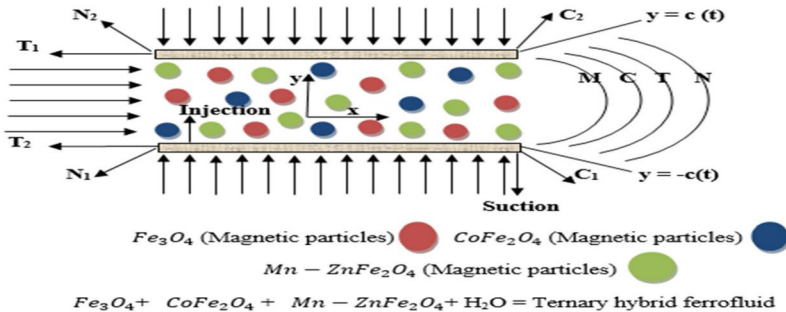


Figure 1. Physical model.

The boundary conditions are,

$$\left. \begin{aligned} y = -c \quad (t)u = 0 \quad v = -Ac'(t)T = T_1, C = C_1, N = N_1 \text{ and} \\ y = c \quad (t)u = 0 \quad v = Ac'(t)T = T_2 \quad T = T_2, C = C_2, N = N_2. \end{aligned} \right\} \quad (7)$$

Temperature variations within a fluid flow are insufficient to allow for a linear formulation of the function T^n . T^n can be extended using Taylor's series for temperature T_2 by omitting higher-order components, yielding the following approximation:

$$\begin{aligned} T^n &= (1-n)T_2^n + nT_2^{n-1}T, \\ \left(\frac{T}{T_2}\right)^n &= (1-n) + n\frac{T}{T_2}. \end{aligned} \quad (8)$$

The derivative $a(t)$ concerning time t is represented by $a'(t)$, where A corresponds to the wall permeability index. Following the removal of the pressure factor from the controlling equation, we apply the transformation of similarities (9) to the aforementioned Eqs. (2–6).

$$\eta = \frac{y}{c}, u = -\frac{\nu_f}{c^2} F_\eta(\eta, t), v = \frac{\nu_f}{c} F(\eta, t), \theta = \frac{T - T_2}{T_1 - T_2}, \chi(\eta) = \frac{C - C_2}{C_1 - C_2}, \psi(\eta) = \frac{N - N_2}{N_1 - N_2} \left. \right\}. \quad (9)$$

The results are,

$$\begin{aligned} \frac{\nu_{trihffd}}{\nu_f} (F_{\eta\eta\eta\eta} - rF_{\eta\eta}) + \alpha(3F_{\eta\eta} + \eta F_{\eta\eta\eta}) + F_\eta F_{\eta\eta} \left(1 + 2\frac{1}{\rho_{trihffd}} F^*\right) - FF_{\eta\eta} - \frac{\rho_f}{\rho_{trihffd}} \\ MF_{\eta\eta} - FF_{\eta\eta\eta} \frac{c^2 F_{\eta\eta t}}{\nu_f} = 0, \end{aligned} \quad (10)$$

$$\begin{aligned} \theta'' + \frac{k_{hffd}}{k_{trihffd}} \frac{k_{ffd}}{k_{hffd}} \frac{k_{bf}}{k_{ffd}} Pr \left((1 - \phi_1 - \phi_2 - \phi_3) + \phi_1 \frac{(\rho_{cp})\rho_1}{(\rho_{cp})_{trihffd}} + \phi_2 \frac{(\rho_{cp})\rho_2}{(\rho_{cp})_{trihffd}} + \phi_3 \frac{(\rho_{cp})\rho_3}{(\rho_{cp})_{trihffd}} \right) (\eta\alpha - Ref)\theta' - \frac{a^2}{\alpha_{trihffd}} \theta_t \\ + (\lambda * \sigma * Pr) \frac{k_{hffd}}{k_{trihffd}} \frac{k_{ffd}}{k_{hffd}} \frac{k_{bf}}{k_{ffd}} (1 + (n*\gamma)\theta[\eta]) (1 - E + (E*\gamma)\theta[\eta]) \chi[\eta] = 0, \end{aligned} \quad (11)$$

$$\chi'' + Sc(\eta\alpha - Ref)\chi' - \frac{a^2}{D} \chi_t + (Sc*\sigma)(1 + (n*\gamma)\theta[\eta]) (1 - E + (E*\gamma)\theta[\eta]) \chi[\eta] = 0, \quad (12)$$

$$(D_n)_{trihffd} \psi'' + \nu_f(\alpha\eta - 2F)\psi' - k^2\psi_t - bW_c(\psi'\chi' + \psi''\chi + N_2\chi'') = 0, \quad (13)$$

With boundary condition

$$\begin{aligned} \eta = -1, F = -Re, F_\eta = 0, \theta = 1, \chi = 1, \psi = 1, \\ \text{and } \eta = 1, F = Re, F_\eta = 0, \theta = 0, \chi = 0, \psi = 0., \end{aligned} \quad (14)$$

Here T_1 and T_2 (with $T_1 > T_2$) are the fixed temperatures of the lower and upper channel C_1 , C_2 , N_1 and N_2 are denotes the concentration and motile microorganisms of upward and downward porous medium respectively, $F = xF'$ Darcy porous medium parameter, $\alpha = \frac{cc'(t)}{\nu_f}$ is the wall expansion ratio, $Re = \frac{Acc'(t)}{\nu_f}$ is the permeability Reynolds number, $r = \frac{c^2}{k^*}$ Porous medium parameter, Eckert number, $Pr = \frac{(\mu_{cp})_f}{k_f}$ Prandtl number. Thermal diffusivity tri hybrid ferrofluid stands for $\alpha_{trihffd} = \frac{k_{trihffd}}{(\rho_{cp})_{trihffd}}$, exothermic/endothermic parameter shown by $\lambda = \frac{\beta(C_1 - C_2)}{(\rho_{cp})(T_1 - T_2)}$, temperature difference parameter represented by $\gamma = \frac{T_1 - T_2}{T_2}$, magnetic field parameter is demonstrated $M = \frac{\sigma_e B_0^2 c^2}{\mu_f}$, the dimensionless reaction rate is shown by $\sigma = \frac{k_r^2(1-\gamma)}{c}$, magnetic field parameter is demonstrated $M = \frac{\sigma_e B_0^2 c^2}{\mu_f}$, $Sc = \frac{\nu_f}{(D_b)_{trihffd}}$ represent the Schmidt number for mass transfer, $Sb = \frac{\nu_f}{(D_n)_{trihffd}}$

represent the Schmidt number for Bio convection, $Pe = \frac{bWc}{(D_n)_{trihffid}}$ is denoted by the Peclet number, $E = \frac{E_a}{k^*T}$ denoted the dimensional activation energy parameter.

Thus, we put $F = f Re$, $G = gRe$ and keeping in view the instance of Majdalani *et al.* [70] in which α is a constant, $f = f(\eta)$, $\theta = \theta(\eta)$, $\chi = \chi(\eta)$, and $\psi = \psi(\eta)$ that process to give $\theta_t = 0$, $f_{\eta t} = 0$, $\chi_t = 0$ and $\psi_t = 0$. Hence the following equations are achieved:

$$\frac{\nu_{trihffid}}{\nu_f} (f_{\eta\eta\eta\eta} - rf_{\eta\eta}) + \alpha(3f_{\eta\eta} + \eta f_{\eta\eta\eta}) + Ref_{\eta} f_{\eta} \left(1 + 2 \frac{1}{\rho_{trihffid}} F \right) - \frac{\rho_f}{\rho_{trihmf}} Mf_{\eta\eta} - Ref_{\eta\eta\eta} = 0, \quad (15)$$

$$\theta_{\eta\eta} + \left((1 - (\varphi_1 + \varphi_2 + \varphi_3)) + (\varphi_1) \left(\frac{\rho_{cps_1}}{\rho_{cpbf}} \right) + (\varphi_2) \left(\frac{\rho_{cps_2}}{\rho_{cpbf}} \right) + (\varphi_3) \left(\frac{\rho_{cps_3}}{\rho_{cpbf}} \right) \right) \left(\frac{k_{hffid}}{k_{trihffid}} \frac{k_{ffd}}{k_{hffid}} \frac{k_{bf}}{k_{ffd}} Pr(\alpha\eta - Ref)\theta_{\eta} \right) + (\lambda*\sigma*Pr) \frac{k_{hffid}}{k_{trihffid}} \frac{k_{ffd}}{k_{hffid}} \frac{k_{bf}}{k_{ffd}} (1 + (n*\gamma)\theta[\eta])(1 - E + (E*\gamma)\theta[\eta])\chi[\eta] = 0, \quad (16)$$

$$\chi'' + Sc(\eta\alpha - Ref)\chi' + (Sc*\sigma)(1 + (n*\gamma)\theta[\eta])(1 - E + (E*\gamma)\theta[\eta])\chi[\eta] = 0, \quad (17)$$

$$(\psi'' + Sb \alpha\eta - 2fRe)\psi' - Pe(\psi'\chi' + \psi''\chi + N_2\chi'') = 0, \quad (18)$$

$$\eta = -1; f = -1, f_{\eta} = 0, \theta = 1, \chi = 1, \psi = 1 \text{ and } \eta = 1; f = 1, f_{\eta} = 0, \theta = 0, \chi = 0, \psi = 0. \quad (19)$$

3. Numerical method

The Runge-Kutta (RK) method is a family of numerical methods used for solving ordinary differential equations (ODEs) and systems of ODEs. It provides a systematic way to approximate the solutions of differential equations by iteratively updating the dependent variable at discrete time steps. The term “shooting technique” likely refers to a technique used to find the appropriate initial conditions for the ODE such that the solution satisfies a specific boundary condition. This is often required when dealing with boundary value problems. In summary, the combination of the Runge-Kutta method and shooting procedures allows for a numerical solution to the differential equation governing the current flow scenario. The RK method handles the time discretization, while shooting procedures help determine the initial conditions for the problem.

3.1. Applying ternary hybrid ferrofluid thermophysical properties convert into numerical modeling

Shape equation numbers (15) and (18) to change the differential equation of nonlinear particles into a pair of highly non-linear ordinary differential equations.

$$\left(\frac{1}{(1 - (\varphi_1 + \varphi_2 + \varphi_3))^{2.5} \left((1 - \varphi_1 - \varphi_2 - \varphi_3) + \varphi_1 \left(\frac{\rho_{s_1}}{\rho_{bf}} \right) + \varphi_2 \left(\frac{\rho_{s_2}}{\rho_{bf}} \right) + (\varphi_3) \left(\frac{\rho_{s_3}}{\rho_{bf}} \right) \right)} \right)$$

$$(f_{\eta\eta\eta\eta} - rf_{\eta\eta}) + \alpha(3f_{\eta\eta} + \eta f_{\eta\eta\eta}) - Ref_{\eta\eta\eta}$$

$$\begin{aligned}
 & + \left(1 + 2 \left(\frac{1}{\left((1 - \varphi_1 - \varphi_2 - \varphi_3) + \varphi_1 \left(\frac{\rho_{s1}}{\rho_{bf}} \right) + \varphi_2 \left(\frac{\rho_{s2}}{\rho_{bf}} \right) + (\varphi_3) \left(\frac{\rho_{s3}}{\rho_{bf}} \right) \right)} \right) F \right) Ref_n f_{\eta\eta} \\
 & - \left(\frac{1}{\left((1 - \varphi_1 - \varphi_2 - \varphi_3) + \varphi_1 \left(\frac{\rho_{s1}}{\rho_{bf}} \right) + \varphi_2 \left(\frac{\rho_{s2}}{\rho_{bf}} \right) + (\varphi_3) \left(\frac{\rho_{s3}}{\rho_{bf}} \right) \right)} \right) Mf''[\eta] = 0, \quad (20) \\
 & \theta''[\eta] + \left((1 - (\varphi_1 + \varphi_2 + \varphi_3)) + (\varphi_1) \left(\frac{\rho_{cps1}}{\rho_{cpbf}} \right) + (\varphi_2) \left(\frac{\rho_{cps2}}{\rho_{cpbf}} \right) + (\varphi_3) \left(\frac{\rho_{cps3}}{\rho_{cpbf}} \right) \right) \\
 & \left(\frac{k_{s3} + (n_3 - 1)k_{hffd} + \varphi_3(k_{hffd} - k_{s3})}{k_{s3} + (n_3 - 1)k_{hffd} - (n_3 - 1)\varphi_3(k_{hffd} - k_{s3})} \right) \left(\frac{k_{s2} + (n_2 - 1)k_{nffd} + \varphi_2(k_{nffd} - k_{s2})}{k_{s2} + (n_2 - 1)k_{nffd} - (n_2 - 1)\varphi_2(k_{nffd} - k_{s2})} \right) \\
 & \left(\frac{k_{s1} + (n_1 - 1)k_{bf} + \varphi_1(k_{bf} - k_{s1})}{k_{s1} + (n_1 - 1)k_{bf} - (n_1 - 1)\varphi_1(k_{bf} - k_{s1})} \right)
 \end{aligned}$$

$$\begin{aligned}
 & \left(Pr(\alpha\eta - Ref[\eta])\theta'[\eta] + \left(\frac{k_{s3} + (n_3 - 1)k_{hffd} + \varphi_3(k_{hffd} - k_{s3})}{k_{s3} + (n_3 - 1)k_{hffd} - (n_3 - 1)\varphi_3(k_{hffd} - k_{s3})} \right) \right. \\
 & \left. \left(\frac{k_{s2} + (n_2 - 1)k_{ffd} + \varphi_2(k_{ffd} - k_{s2})}{k_{s2} + (n_2 - 1)k_{ffd} - (n_2 - 1)\varphi_2(k_{ffd} - k_{s2})} \right) \right. \\
 & \left. \left(\frac{k_{s1} + (n_1 - 1)k_{bf} + \varphi_1(k_{bf} - k_{s1})}{k_{s1} + (n_1 - 1)k_{bf} - (n_1 - 1)\varphi_1(k_{bf} - k_{s1})} \right) (Pr*\sigma * \lambda) \right) \\
 & \left((1 + (\gamma*n)\theta[\eta])(1 - E + (\gamma*E)\theta[\eta])\chi[\eta] = 0, \quad (21)
 \end{aligned}$$

$$\chi'' + Sn(\eta\alpha - Ref)\chi' + (Sc*\sigma)(1 + (n*\gamma)\theta[\eta])(1 - E + (E*\gamma)\theta[\eta])\chi[\eta] = 0, \quad (22)$$

$$\psi'' + Sb(\alpha\eta - 2fRe)\psi' - Pe(\psi'\chi' + \psi''\chi + N_2\chi'') = 0, \quad (23)$$

$$W_1 = \left(\frac{1}{(1 - (\varphi_1 + \varphi_2 + \varphi_3))^{2.5} \left((1 - \varphi_1 - \varphi_2 - \varphi_3) + \varphi_1 \left(\frac{\rho_{s1}}{\rho_{bf}} \right) + \varphi_2 \left(\frac{\rho_{s2}}{\rho_{bf}} \right) + (\varphi_3) \left(\frac{\rho_{s3}}{\rho_{bf}} \right) \right)} \right), \quad (24)$$

$$W_2 = \left(\frac{1}{\left((1 - \varphi_1 - \varphi_2 - \varphi_3) + \varphi_1 \left(\frac{\rho_{s1}}{\rho_{bf}} \right) + \varphi_2 \left(\frac{\rho_{s2}}{\rho_{bf}} \right) + (\varphi_3) \left(\frac{\rho_{s3}}{\rho_{bf}} \right) \right)} \right), \quad (25)$$

$$W_3 = \left((1 - \varphi_1 - \varphi_2 - \varphi_3) + \varphi_1 \left(\frac{\rho_{s1}}{\rho_{bf}} \right) + \varphi_2 \left(\frac{\rho_{s2}}{\rho_{bf}} \right) + (\varphi_3) \left(\frac{\rho_{s3}}{\rho_{bf}} \right) \right), \quad (26)$$

$$W_4 = \left(\frac{k_{s3} + (n_3 - 1)k_{hffd} + \varphi_3(k_{hffd} - k_{s3})}{k_{s3} + (n_3 - 1)k_{hffd} - (n_3 - 1)\varphi_3(k_{hffd} - k_{s3})} \right), \quad (27)$$

$$W_5 = \left(\frac{k_{s2} + (n_2 - 1)k_{ffd} + \varphi_2(k_{ffd} - k_{s2})}{k_{s2} + (n_2 - 1)k_{ffd} - (n_2 - 1)\varphi_2(k_{ffd} - k_{s2})} \right), \tag{28}$$

$$W_6 = \left(\frac{k_{s1} + (n_1 - 1)k_{bf} + \varphi_1(k_{bf} - k_{s1})}{k_{s1} + (n_1 - 1)k_{bf} - (n_1 - 1)\varphi_1(k_{bf} - k_{s1})} \right), \tag{29}$$

$$B = W_4 W_5 W_6, \tag{30}$$

When the values (24), (25), (26), (27), (28), (29), and (30) are entered into Eqs. (20, 23), the outcome is

$$W_1(f_{\eta\eta\eta\eta} - rf_{\eta\eta}) + \alpha(3f_{\eta\eta} + \eta f_{\eta\eta\eta}) + Ref_{\eta}f_{\eta\eta}(1 + 2W_2 F) - Ref_{\eta\eta\eta} - MW_2f''[\eta] = 0, \tag{31}$$

$$\theta''[\eta] + W_3B(Pr(\alpha\eta - Ref[\eta])\theta'[\eta] + (Pr*\sigma * \lambda)B((1 + (\gamma*n)\theta[\eta])(1 - E + (\gamma*E)\theta[\eta])\chi[\eta]) = 0, \tag{32}$$

$$\chi'' + Sc(\eta\alpha - Ref)\chi' + (Sc*\sigma)(1 + (n*\gamma)\theta[\eta])(1 - E + (E*\gamma)\theta[\eta])\chi[\eta] = 0, \tag{33}$$

$$\psi'' + Sb(\alpha\eta - 2fRe)\psi' - Pe(\psi'\chi' + \psi''\chi + N_2\chi'') = 0. \tag{34}$$

3.2. Solution of the problem

To start the procedure, the following changes must be made:

$$r_1 = f[\eta], r_2 = f'[\eta], r_3 = f''[\eta], r_4 = f'''[\eta], r_5 = \theta[\eta], r_6 = \theta'[\eta], r_7 = \chi[\eta], r_8 = \chi'[\eta], r_9 = \psi[\eta], r_{10} = \psi'[\eta]. \tag{35}$$

Lastly, alter the model as given in Eqs. (31–35).

$$f''''[\eta] = \frac{1}{W_1} \left(-\alpha(3f''[\eta] + \eta f''''[\eta]) + Ref[\eta]f''''[\eta] + rf''[\eta] - (1 + 2W_2F^*)Ref'[\eta]f''[\eta] - MW_2f''[\eta] \right), \tag{36}$$

$$\theta''[\eta] = -(W_3BPr(\alpha\eta - 2Ref[\eta])\theta'[\eta] + (\lambda*\sigma*Pr)B(1 + (n*r)\theta[\eta])(1 - E + (E*r)\theta[\eta])\chi[\eta]), \tag{37}$$

$$\chi''[\eta] = -(Sc(\eta\alpha - Ref)\chi'[\eta] + (Sc*\sigma)(1 + (n*\gamma)\theta[\eta])(1 - E + (E*\gamma)\theta[\eta])\chi[\eta]), \tag{38}$$

$$\psi''[\eta] = Sb(-\alpha\eta + 2fRe)\psi'[\eta] + Pe(\psi'[\eta]\chi'[\eta] + \psi''[\eta]\chi[\eta] + N_2\chi''[\eta]), \tag{39}$$

The following system is obtained by employing the replacement contained in Eq. (35):

$$\begin{bmatrix} r_1^{*f} \\ r_2^{*f} \\ r_3^{*f} \\ r_4^{*f} \\ r_5^{*f} \\ r_6^{*f} \\ r_7^{*f} \\ r_8^{*f} \\ r_9^{*f} \\ r_{10}^{*f} \end{bmatrix} = \begin{bmatrix} r_2 \\ r_3 \\ r_4 \\ \frac{1}{W_1}(-\alpha(3r_3 + \eta r_4) + Re(r_1 r_4) + r r_3 + Re(1 + 2W_2F^*)r_2 r_3 - MW_2 r_3) \\ r_6 \\ -(W_3BPr(\alpha\eta - 2Rer_1)r_6 + (\lambda * \sigma * Pr)B(1 + (n * r)r_5)(1 - E + (E * r)r_5)r_7) \\ r_7 \\ -(Sc(\eta\alpha - Rer_1)r_7 + (Sc*\sigma)(1 + (n*\gamma)r_6)(1 - E + (E*\gamma)r_6)r_7) \\ r_9 \\ Sb(-\alpha\eta + 2Rer_1)_{10} + Pe(r_{10}r_8 + \psi''r_7 + N_2\chi'') \end{bmatrix}.$$

Consequently, the initial condition is:

$$\begin{bmatrix} r_1^* \\ r_2^* \\ r_3^* \\ r_4^* \\ r_5^* \\ r_6^* \\ r_7^* \\ r_8^* \\ r_9^* \\ r_{10}^* \end{bmatrix} = \begin{bmatrix} -1 \\ 0 \\ 1 \\ 0 \\ 1 \\ 0 \\ 1 \\ 0 \\ 1 \\ 0 \end{bmatrix}. \quad (40)$$

The aforementioned problem is now solved using mathematics and a correct starting condition. Both the RK approach and the numerical “shooting technique” were explored in this scenario. This approach simplifies the processing of the required dimensionless ordinary differential equations. In the beginning, we employ the shooting strategy to establish the starting state, making sure that the border conditions are satisfied and that the requisite degree of accuracy is obtained.

3.3. Practical and engineering interests

In upper and lower porous mediums all variables are investigated including the physical parameters that are required in engineering to represent equipment at the nano level as Skin friction, Nusselt number, Sherwood number, and Motile number.

3.3.1. Skin friction coefficients

Permeable porous medium upward and downward skin friction coefficients are represented by C_{f1} and C_{f-1} expressed as

$$C_{f-1} = \frac{\zeta_y|_{\eta=-1}}{\rho_f(c'A)^2} = \frac{1}{Re_r(1 - \varphi_1 - \varphi_2)^{2.5}} f''(-1), \quad (41)$$

$$C_{f1} = \frac{\zeta_y|_{\eta=1}}{\rho_f(c'A)^2} = \frac{1}{Re_r(1 - \varphi_1 - \varphi_2)^{2.5}} f''(1).$$

local Reynolds numbers are shown by $Re_r = \left(\frac{c}{r}\right) \frac{1}{(Re)^2}$ or the upper and lower shear stress porous medium in radial velocity direction

$$\zeta_y = \mu_{trihfd} \left(\frac{\partial u}{\partial y} \right) \Big|_{\eta = -1} = \frac{\mu_{bf}}{(1 - \varphi_1 - \varphi_2 - \varphi_3)^{2.5}} \left(\frac{rv_f}{c^3} \right) f''(-1),$$

$$\zeta_y = \mu_{trihfd} \left(\frac{\partial u}{\partial y} \right) \Big|_{\eta = 1} = \frac{\mu_{bf}}{(1 - \varphi_1 - \varphi_2 - \varphi_3)^{2.5}} \left(\frac{rv_f}{c^3} \right) f''(1),$$

3.3.2. Nusselt number

The flow of heat transfer rate in the below and top porous medium Nusselt number is demonstrated by Nu_{y-1} and Nu_{y1} are given as

$$\begin{aligned}
 Nu_{y,-1} &= \frac{cd_y}{\kappa_f(T_1 - T_2)} \Big|_{\eta=-1} = -\frac{k_{trihffd}}{k_f} \theta'(-1), \\
 Nu_{y,1} &= \frac{cd_y}{\kappa_f(T_1 - T_2)} \Big|_{\eta=1} = -\frac{k_{trihffd}}{k_f} \theta'(1).
 \end{aligned} \tag{42}$$

d_y stand for heat flux is follows as

$$\begin{aligned}
 d_y \Big|_{\eta=-1} &= -k_{trihffd} \left(\frac{\partial T}{\partial y} \right) \Big|_{\eta=-1} = -\frac{(T_1 - T_2)}{c} k_{trihffd} \theta'(-1), \\
 d_y \Big|_{\eta=1} &= -k_{trihffd} \left(\frac{\partial T}{\partial y} \right) \Big|_{\eta=1} = -\frac{(T_1 - T_2)}{c} k_{trihffd} \theta'(1),
 \end{aligned}$$

3.3.3. Sherwood number

The proportion of diffused mass transfer to convectonal mass transmission is known as the Sherwood number. The rate of mass transfer (Sherwood number) $Sh \Big|_{\eta=-1}$ as well as $Sh \Big|_{\eta=1}$ at the top and bottom surfaces of the surface contain the said mathematical equation,

$$\begin{aligned}
 Sh \Big|_{\eta=-1} &= \frac{kq_z}{(D_b)_{trihffd}(C_1 - C_2)} \Big|_{\eta=-1} = -\chi'(-1), \\
 Sh \Big|_{\eta=1} &= \frac{kq_z}{(D_b)_{trihffd}(C_1 - C_2)} \Big|_{\eta=1} = -\chi'(1).
 \end{aligned} \tag{43}$$

Where

$$\begin{aligned}
 q_z \Big|_{\eta=-1} &= -(D_b)_{trihffd} \left(\frac{\partial C}{\partial z} \right) \Big|_{\eta=-1} = -(D_b)_{trihffd} \frac{(C_1 - C_2)}{k} \chi'(-1), \\
 q_z \Big|_{\eta=1} &= -(D_b)_{trihffd} \left(\frac{\partial C}{\partial z} \right) \Big|_{\eta=1} = -(D_b)_{trihffd} \frac{(C_1 - C_2)}{k} \chi'(1),
 \end{aligned}$$

3.3.4. Motile density number

Both porous surfaces are represented by $Nn \Big|_{\eta=-1}$ and $Nn \Big|_{\eta=1}$ of motile number are expressed as

$$\begin{aligned}
 Nn \Big|_{\eta=-1} &= \frac{kq_n}{(D_n)_{trihffd}(N_1 - N_2)} \Big|_{\eta=-1} = -\psi'(-1), \\
 Nn \Big|_{\eta=1} &= \frac{kq_n}{(D_n)_{trihffd}(N_1 - N_2)} \Big|_{\eta=1} = -\psi'(1).
 \end{aligned} \tag{44}$$

Here

$$\begin{aligned}
 q_z \Big|_{\eta=-1} &= -(D_n)_{trihffd} \left(\frac{\partial N}{\partial z} \right) \Big|_{\eta=-1} = -(D_n)_{trihffd} \frac{(N_1 - N_2)}{k} \psi'(-1), \\
 q_z \Big|_{\eta=1} &= -(D_n)_{trihffd} \left(\frac{\partial N}{\partial z} \right) \Big|_{\eta=1} = -(D_n)_{trihffd} \frac{(N_1 - N_2)}{k} \psi'(1),
 \end{aligned}$$

4. Results and discussion

In this mathematical model research, the finally transformed Eqs. (30–33) are derived to establish a nonlinear boundary problem. The analytical solution for such equations is difficult to obtain so to solve this a numerical approach is used which is the application of the Runge–Kutta method. The effects of related physical factors Peclet number, magnetic field, Prandtl number, Reynolds number, the volume of friction, density ratio motile microorganisms, shape factor, Schmidt number, expansion ratio parameter regarding velocity, temperature, concentration, as well as mobile microorganisms are shown in Figures (2–18). The numeric impact of these physical parameters is shown in Tables (1–5). Table 1 represents the base fluid (water) and different types of magnetic ferrofluid particles and Table 2 shows the thermophysical properties of ternary hybrid ferrofluid. It can be seen from Table 3 that the value of the skin friction coefficient varies but Reynold’s number is fixed. First of all, if Reynold’s number is less than the values of Darcy porous medium (F), porous medium (r), and magnetic parameter then the flow of skin friction is enhanced in both porous surfaces but the expansion ratio (α) values are lies form – ve to + ve so flow of shear stress is reduced in the upper and lower porous surface. Furthermore, Reynold’s numbers

Table 1. Different magnetic nanoparticles and base fluid thermophysical properties.

Title	H ₂ O (bf)	Fe ₃ O ₄ (φ_1)	CoFe ₂ O ₄ (φ_2)	Mn – ZnFe ₂ O ₄ (φ_3)
ρ (kg m ⁻³)	997.0	5180	4907	4900
C_p (J k g ⁻¹ k ⁻¹)	4180	670	700	800
κ (wm ⁻¹ k ⁻¹)	0.6071	9.7	3.7	5

Table 2. Tri-hybrid ferrofluid thermophysical properties.

Properties	Trihfffd	Fe ₃ O ₄ + CoFe ₂ O ₄ + Mn – ZnFe ₂ O ₄ /water
Density (kgm ⁻³)	$\rho_{trihfffd} = \varphi_1\rho_{s_1} + \varphi_2\rho_{s_2} + \varphi_3\rho_{s_3} - (1 - \varphi_1 - \varphi_2 - \varphi_3)\rho_{bf}$	
Heat capacity (JK ⁻¹)	$(\rho C_p)_{trihfffd} = \varphi_1(\rho C_p)_{s_1} + \varphi_2(\rho C_p)_{s_2} + \varphi_3(\rho C_p)_{s_3} + (1 - \varphi_1 - \varphi_2 - \varphi_3)(\rho C_p)_{bf}$	
Viscosity (Nsm ⁻¹)	$\mu_{trihfffd} = \frac{\mu_{bf}}{(1-\varphi_1-\varphi_2-\varphi_3)^{2.5}}$	
Thermal Conductivity k (Wk ⁻¹ m ⁻¹)	$k_{trihfffd} = \frac{k_{s3}+(n_3-1)k_{hfffd}-(n_3-1)\varphi_3(k_{hfffd}-k_{s3})}{k_{s3}+(n_3-1)k_{hfffd}+\varphi_3(k_{hfffd}-k_{s3})} k_{hfffd}$ $k_{hfffd} = \frac{k_{s2}+(n_2-1)k_{fffd}-(n_2-1)\varphi_2(k_{fffd}-k_{s2})}{k_{s2}+(n_2-1)k_{fffd}+\varphi_2(k_{fffd}-k_{s2})} k_{fffd}$	
Where	$k_{fffd} = \frac{k_{s1}+(n_1-1)k_{bf}-(n_1-1)\varphi_1(k_{bf}-k_{s1})}{k_{s1}+(n_1-1)k_{bf}+\varphi_1(k_{bf}-k_{s1})} k_{bf}$	

Table 3. Numerical effect in skin friction coefficient for both porous medium on Darcy porous medium (F), porous medium parameter (r), and magnetic field parameter (M) for tri hybrid ferrofluid (Fe₃O₄+ CoFe₂O₄ + Mn – ZnFe₂O₄/water).

F	r	M	α	$Re = -1/2$		$Re = 1/2$	
				$ C_{f(\eta=-1)} $	$ C_{f(\eta=1)} $	$ C_{f(\eta=-1)} $	$ C_{f(\eta=1)} $
1	1	1	1	2.5521	2.5521	2.2029	2.2029
2				2.6878	2.6878	1.9947	1.9947
3				2.8169	2.8169	1.7643	1.7643
4				2.9403	2.9403	1.5052	1.5052
	1.5			2.6406	2.6406	2.3212	2.3212
	2			2.7271	2.7271	2.4353	2.4353
	2.5			2.8116	2.8116	2.5456	2.5456
	3			2.8943	2.8943	2.6523	2.6523
		3		2.6751	2.6751	2.4686	2.4686
		5		2.7323	2.7323	2.5415	2.5415
		7		2.7886	2.7886	2.6127	2.6127
		9		2.8441	2.8441	2.6825	2.6825
			-0.5	3.7879	3.7879	3.7972	3.7972
			0	3.4564	3.4564	3.4094	3.4094
			0.5	3.1958	3.1958	3.1039	3.1039
			1	2.8441	2.8441	2.6825	2.6825

are fixed and greater than zero therefore the flow of skin friction coefficient acts opposite on F , α , r and M in both porous surfaces.

Table 4 shows that with the increases in the rate of Activation energy (E), the flow of the Nusselt number is enhanced but the flow of the Sherwood number acts vice versa in both porous mediums. Enhance the values of dimensionless reaction ratio (σ), density ratio of motile number, and similarity variable parameter the flow of upward and downward Nusselt and Sherwood number are numerical effect show in opposite. Furthermore, by growing the values of Reynold number and expansion ratio parameter the flow of energy transfer acted vice versa but the flow of mass transfer are gradually enhanced in both porous medium. From Table 5, it is clear that by raising the Schmidt number (Sc) while keeping the Peclet number (Pe) and density ratio (γ) constant, the density of Motile microorganisms for both porous disks decreases so varies inversely. Also, if the value Pe is increased while keeping Sc and γ constant, the Motile microorganisms' density for the upper permeable disk is decreased while in lower porous it is increased. Now the same calculations are being done while increasing the value of γ and keeping Sc and Pe constant. The results show that the density of Motile microorganisms for both porous disks decrease and varies inversely with the increasing value of γ . We validated our findings by comparing them with results from previously published research articles Quershi *et al.* [71] using Table 6 before

Table 4. Nusslet and Sherwood Number effect on different dimensionless parameters on both porous medium in ternary hybrid ferrofluid.

E	σ	γ	n	Re	α	$ Nu _{\eta=-1}$	$ Nu _{\eta=1}$	$ Sh _{\eta=-1}$	$ Sh _{\eta=1}$
1	0.3	0.1	0.5	0.5	-0.5	3.4438	2.3391	0.69423	0.71597
2						15.776	9.2149	0.98364	0.5448
3						25.477	18.071	1.2185	0.42511
	0.4					3.5971	2.2008	0.69008	0.71786
	0.5					1.0499	4.5572	0.66899	0.73143
	0.6					0.37027	5.1978	0.65534	0.73993
		0.2				4.09701	1.7581	0.67517	0.72396
		0.3				1.6147	5.8189	0.59854	0.74187
		0.4				0.26735	7.6542	0.58203	0.76895
			0.6			3.4459	2.3373	0.6941	0.7161
			0.7			1.9727	3.6927	0.68839	0.71992
			0.8			1.96551	3.6994	0.68822	0.72001
				0.6		4.1496	2.5301	0.72078	0.74184
				0.7		0.7383	6.7266	0.73359	0.77851
				0.8		3.987	12.329	0.74279	0.81921
					-0.6	1.9736	4.0851	0.70945	0.74249
					-0.7	1.8971	4.5604	0.7304	0.76593
					-0.8	1.7283	5.1333	0.75147	0.79016

Table 5. Motile microorganisms the effect of Schmidt number of motile density (Sb), Peclet number (Pe), and motile density ratio parameter (γ) for both porous mediums.

Sb	Pe	γ	$ Nm _{\eta=-1}$	$ Nm _{\eta=1}$
0.2	0.5	2	0.52419	0.28903
0.4			0.35885	0.2247
0.6			0.22276	0.1675
0.8			0.11305	0.1172
0.2	0.6		0.54596	0.25264
	0.7		0.57345	0.21468
	0.8		0.61073	0.17469
	0.9		0.67007	0.13173
	0.5	2.2	0.51603	0.2848
		2.4	0.50786	0.28058
		2.6	0.49978	0.27635
		2.8	0.49153	0.27212

visualizing the outcomes. An excellent coincidence was observed, confirming the method's validity.

It can be observed from [Figure 2](#) that the Expanding/Contracting ratio parameter (α) affects the radial velocity profile. The graphic shows that the momentum border layer thickness amount is the smallest on the lower and upper porous surface of plates and maximum at the center of the surface. [Figure 3](#) reveals that the concentration profile is dependent on the Expanding/Contracting ratio parameter (α) while the physical parameters such as Reynold number (Re), volume fraction ($\varphi_1, \varphi_2, \varphi_3$), the diameter of nanoparticles (dp_1, dp_2 and dp_3) and Magnetic flux parameter (M) constant. The value of the mass transfer is highest at the top porous plane of the plate and depleted at the lower porous surface of the plate. The analysis shown in [Figure 4](#) exhibits the effect of α on the motile profile. The value of the motile profile is high on the upper porous surface of the plate and keeps decreasing at the center of the plate and the minimum value is at the lower porous surface of the plate. [Figure 5](#) illustrates the influence of the magnetic field (M) on the radial velocity outline. The radial velocity profile is at the lowest value at both porous surfaces of plates and peaks in the middle of the wall. [Figure 6](#) shows the effect of Darcy porous material parameter and porous material parameter when varies from positive in the axial velocity profile. If we increase the values of F , then momentum boundary layer thickness also shows a gradually increasing trend at the wall center of the upper permeable surface. The use of permeable materials is intended to improve fluid resistance physically. Movement; reduces the thickness of the boundary layer as well as flow viscosity and momentum. According to [Figure 7](#), if we raise the influence of the Darcy permeable material parameter F over the radial velocity profile, the thickness of the border layer at the core of the wall flow of momentum will decrease, while the top, as well as bottom porous flow of velocity, will rise. The values of the porous medium parameter (r) are shown in [Figure 8](#) to be lying between negative and positive on the radial velocity gradient. The flow of the momentum border layer is rising in both porous materials, while the flow of tri-hybrid ferrofluid in the middle of the wall is very low.

From [Figure 9](#), it can be concluded that the Exothermic/endothermic parameter (λ) impacts the temperature profile. The diagram reveals that the value temperature profile parameter

Table 6. Evaluating the heat and mass transfer rates at the lower porous surface, a comparison of results is conducted for the conditions of $Re = 0, E = 0, n = 0, Pr = 0,$ and $M = 0$.

α	Quershi <i>et al.</i> [73]		Present Results	
	$\theta(-1)$	$\chi(-1)$	$\theta(-1)$	$\chi(-1)$
-1.5	1.80925	0.84674	1.80927	0.84676
-1	0.94617	0.62276	0.94620	0.62279
0	0.16084	0.31088	0.16087	0.31090
1.5	0.00558	0.14104	0.00561	0.14106

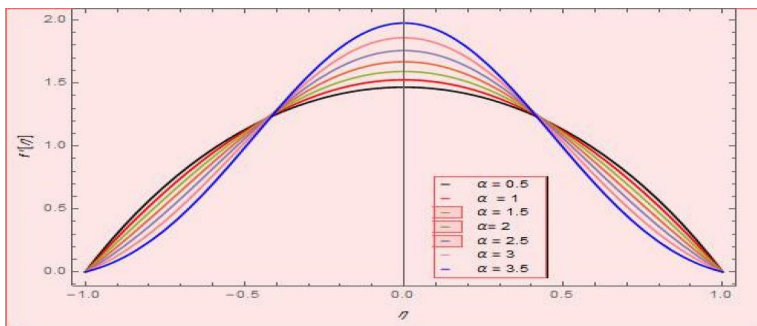


Figure 2. Expanding/contracting ratio parameter α effect on radial velocity profile for $Re = 1, \varphi_1 = \varphi_2 = \varphi_3 = 0.02, dp_1 = dp_2 = dp_3 = 1, M = 4$.

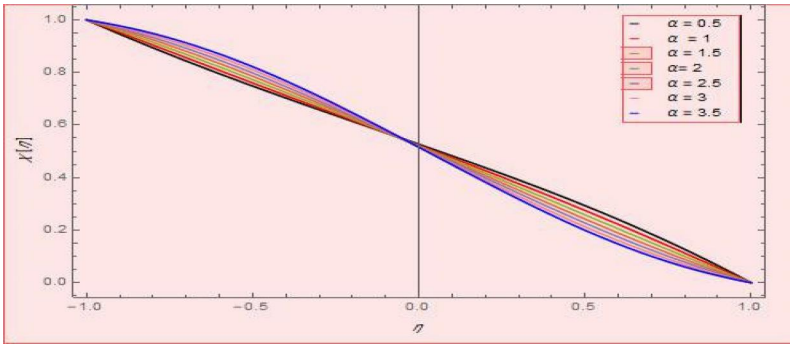


Figure 3. Expanding/contracting ratio parameter α effect on concentration profile for $Re = 1, \varphi_1 = \varphi_2 = \varphi_3 = 0.02, dp_1 = dp_2 = dp_3 = 1, M = 4$.

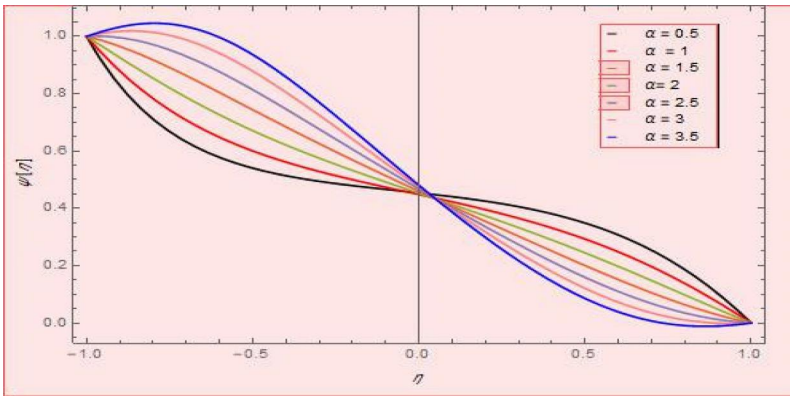


Figure 4. Expanding/contracting ratio parameter α effect on motile profile for $Re = 1, \varphi_1 = \varphi_2 = \varphi_3 = 0.02, dp_1 = dp_2 = dp_3 = 1, M = 4$.

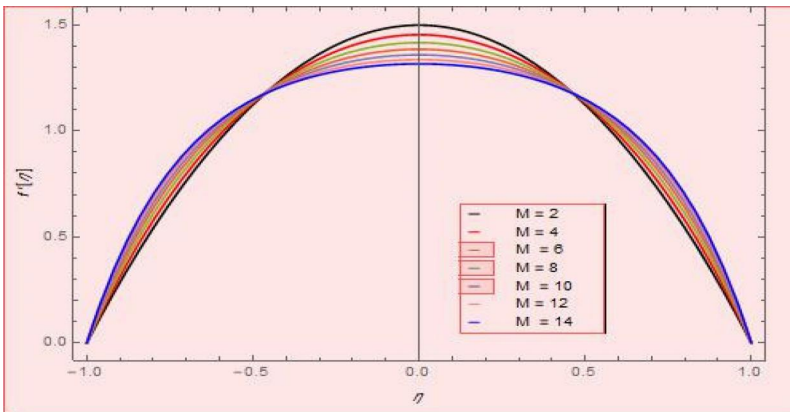


Figure 5. Magnetic field M effect on radial velocity profile for $Re = 1, \varphi_1 = \varphi_2 = \varphi_3 = 0.01, dp_1 = dp_2 = dp_3 = 1, \alpha = 1$.

increases as it approaches from the lower porous plate to the middle of the wall and it reaches the lowest value at the upper porous surface of the plate. The temperature gradient also seems to be affected by the change in the Dimensionless reaction rate parameter (σ) as shown in [Figure 10](#). The border layer thickness of heat is less at the both porous surface of the plate and more in the middle of the wall at various values of σ . [Figure 11](#) clarifies the effect of the

Similarity variable parameter (n) on the thermal border layer thickness of motile microorganisms. As seen from the diagram the border layer thickness of heat rises as we move from the lower porous surface of the plate to the middle of the wall but it decreases as we approach the upper porous surface of the plate. It can be derived from Figure 12 that the temperature profile is affected by the variation in Activation energy (E) while keeping the physical parameters such as Reynold number (Re), volume fraction ($\varphi_1, \varphi_2, \varphi_3$), Prandtl number (Pr), Exothermic/

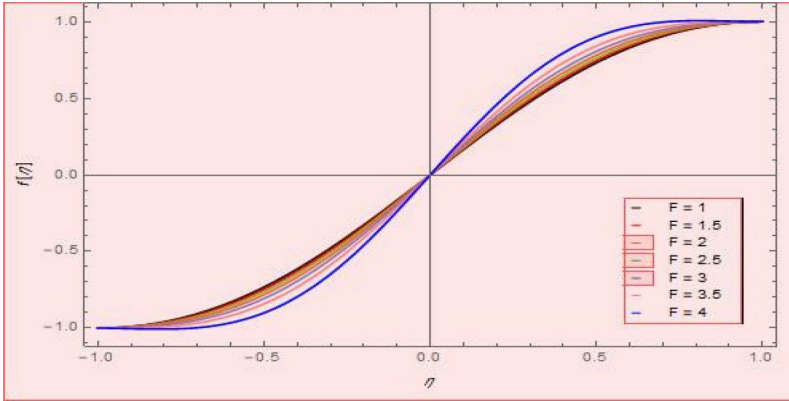


Figure 6. Impact of axial velocity profile on Darcy porous medium parameter (F) for $\alpha = r = Re = 1, \varphi_1 = \varphi_2 = \varphi_3 = 0.01$.

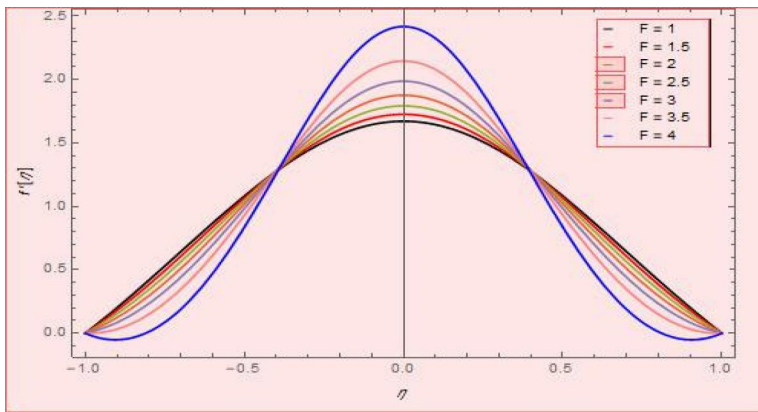


Figure 7. Impact of radial velocity profile on Darcy porous medium parameter (F) for $\alpha = r = Re = 1, \varphi_1 = \varphi_2 = \varphi_3 = 0.01$.

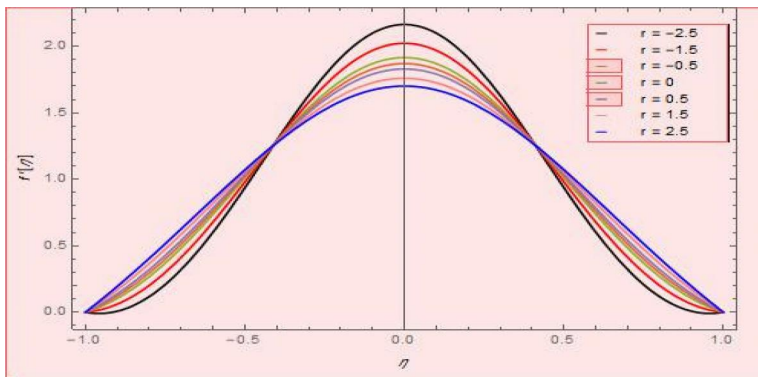


Figure 8. Porous medium parameter (r) effect on radial velocity profile for $\alpha = 2, F = 2, Re = 1, \varphi_1 = \varphi_2 = \varphi_3 = 0.01$.

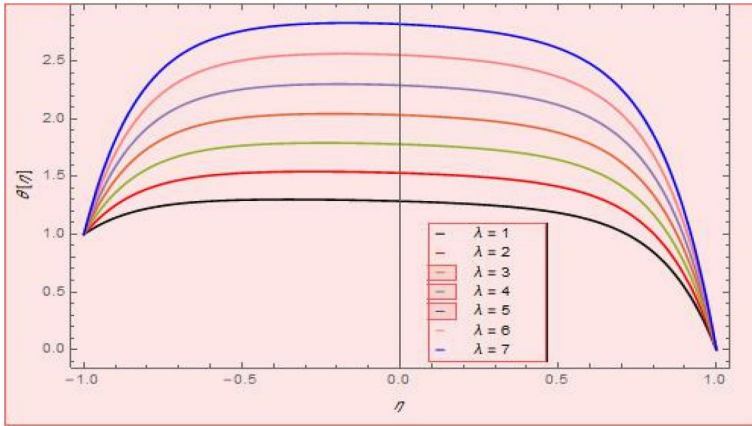


Figure 9. Exothermic/endothermic parameter λ effect on a temperature profile for $Re = 1, \varphi_1 = \varphi_2 = \varphi_3 = 0.02, Pr = 6.2, \sigma = 0.1, n = 0.1, \alpha = 1$.

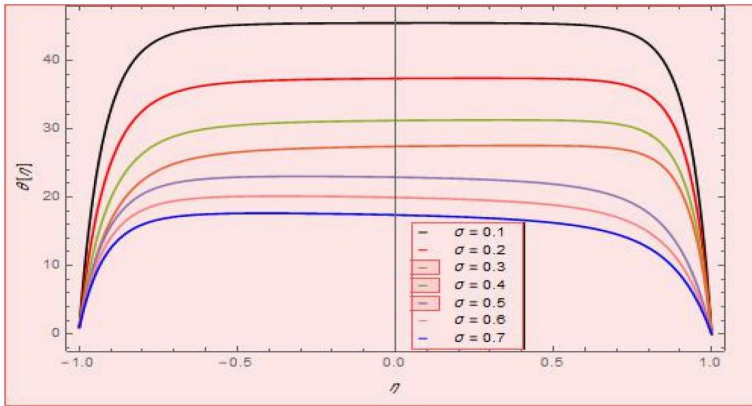


Figure 10. Dimensionless reaction rate parameter σ effect on a temperature profile for $Re = 1, \varphi_1 = \varphi_2 = \varphi_3 = 0.02, Pr = 6.2, \lambda = 1, n = 0.1, E = 0.5, \alpha = -1$.

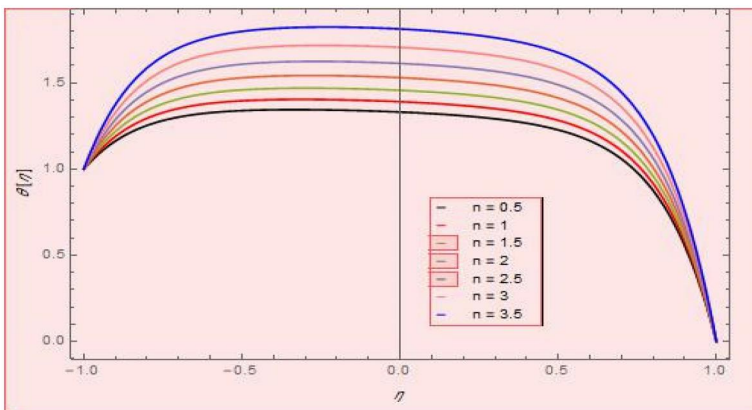


Figure 11. Similarity variable parameter (n) effect on a temperature profile for $Re = 1, \varphi_1 = \varphi_2 = \varphi_3 = 0.02, Pr = 6.2, \lambda = 1, E = 0.5, \sigma = 0.1, \alpha = 1$.

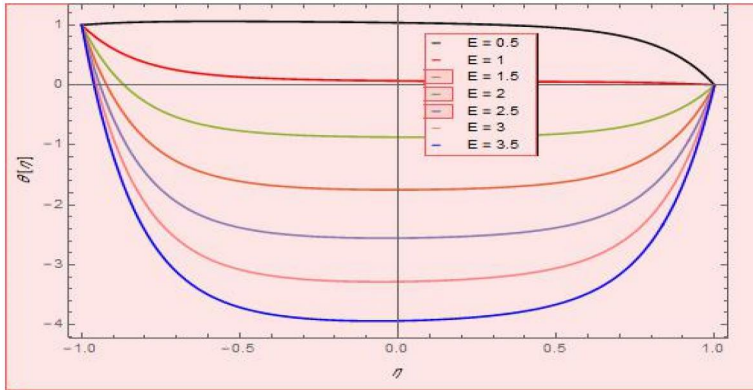


Figure 12. Activation energy (E) effect on a temperature profile for $Re = 1, \varphi_1 = \varphi_2 = \varphi_3 = 0.02, Pr = 6.2, \lambda = 1, n = 0.5, \sigma = 0.1, \alpha = 1$.

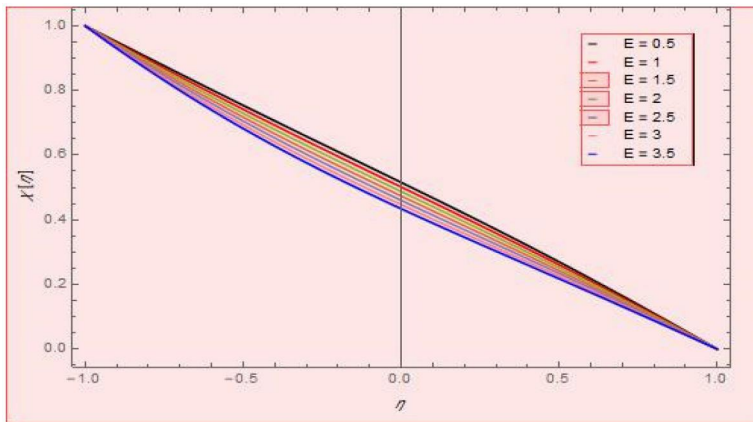


Figure 13. Activation energy (E) effect on concentration profile for $Re = 1, Pr = 6.2, \lambda = 1, n = 0.5, \sigma = 0.1, \alpha = 1$.

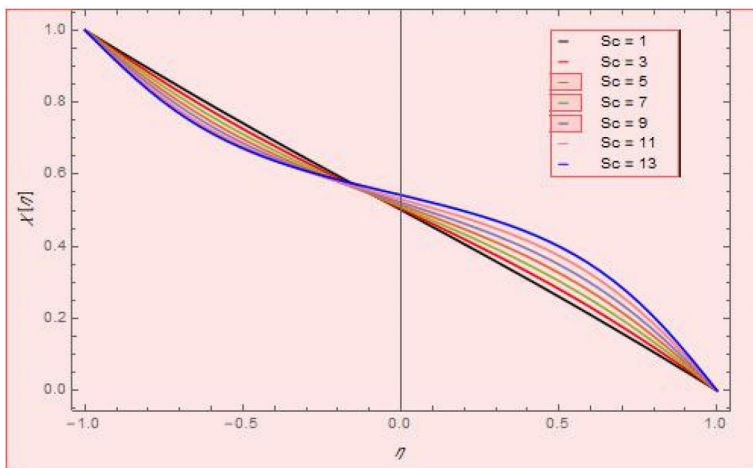


Figure 14. Schmidt number for mass transfer (Sc) effect on concentration profile for $Re = 1, E = 1, \lambda = 1, n = 0.5, \sigma = 0.1, \alpha = 1$.

endothermic parameter (λ), Similarity variable parameter (n), Dimensionless reaction rate parameter (σ), and Expanding/Contracting ratio parameter (α) as constant. The thermal boundary layer thickness at the lower porous surface of the plate is higher in comparison to the upper porous surface. In Figure 13, it can be seen that Activation energy (E) also affects the Concentration

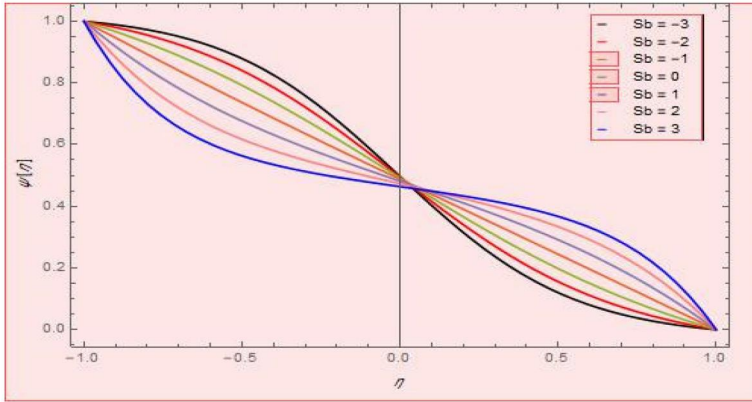


Figure 15. Schmidt number for bioconvection (S_b) effect on motile profile for $Re = 1, Pe = 0.1, N_2 = 4, \alpha = 1$.

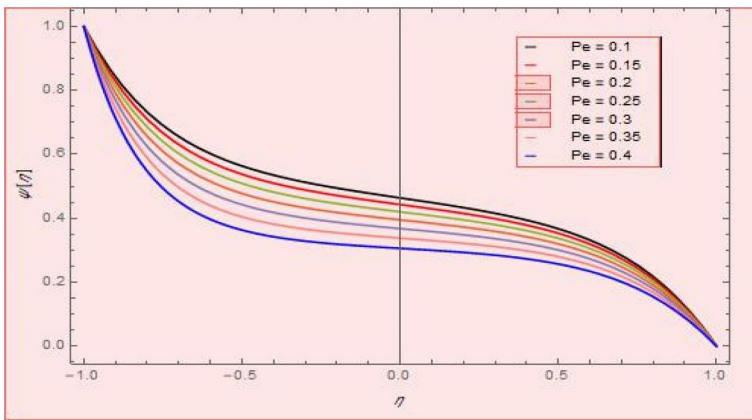


Figure 16. Peclet number (Pe) effect on motile profile for $Re = 1, Pe = 0.1, N_2 = 4, \alpha = 1$.

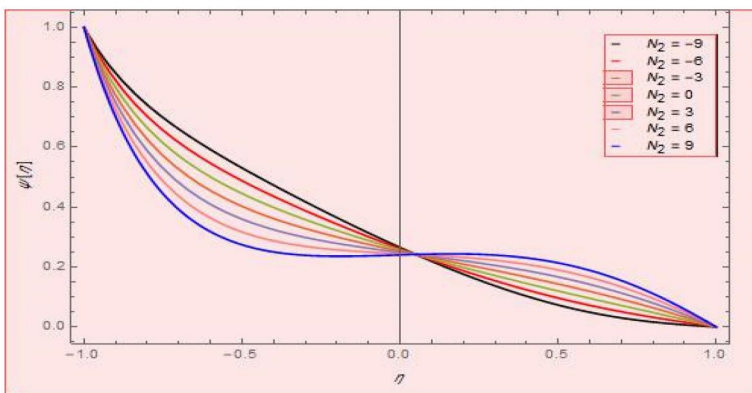


Figure 17. Chemical reaction parameter (N_2) effect on Motile profile for $Re = 1, Pe = 0.7, S_b = 1, \alpha = 1$.

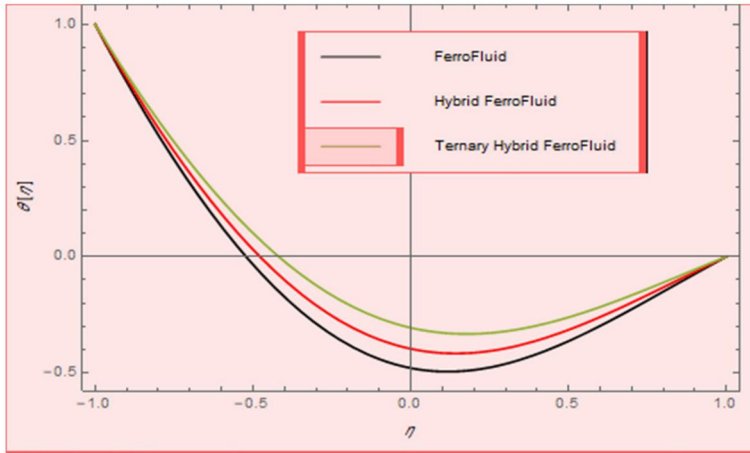


Figure 18. Different magnetic nanoparticles comparison effect on a temperature profile for $Re = 1, Pe = 0.7, Sb = 1, \alpha = 1$.

profile. The value of the concentration profile is the highest at the lower porous area of the plate and minimum at the topside porous area of the plate. The pattern shows symmetrical flow.

Figure 14 describes the effect of varying Schmidt numbers (Sc) for mass transfer on the concentration profile. The highest value of the concentration profile is observed at the bottom side porous surface while the lowest value is observed at the upper porous surface of the plate. From Figure 15, it can be noted that a change in the Schmidt number for Bioconvection (Sb) causes a change in the Motile profile. The results of this change are obtained at the constant values of physical parameters ($Re = 1, Pe = 0.1, N_2 = 4, \alpha = 1$). The Motile profile value is at its peak value at the lower porous surface while the minimum value is observed at the upper porous surface. The motile profile shown in Figure 16 exhibits its dependency on the Peclet number (Pe). As the flow moves from the lower porous surface to the upper porous surface, the value of the motile profile also decreases. So the maximum value is observed at the lower porous surface and the minimum at the upper porous surface of the plate. The Chemical Reaction parameter (N_2) also have an impact on the motile microorganism profile which is evident from Figure 17. The lower porous surface has the peak value of the motile microorganisms profile and as flow moves toward the upper porous surface the value of the profile diminishes. Figure 18 explains the comparison of Nano ferrofluid (Fe_3O_4 /water), hybrid ferrofluid ($Fe_3O_4 + CoFe_2O_4$ /water) and ternary hybrid ferrofluid ($Fe_3O_4 + CoFe_2O_4 + Mn - ZnFe_2O_4$ /water) on the thermal profile. The flow of heat transfer rate is much better in ternary hybrid ferrofluid as compared to nano ferrofluid and hybrid ferrofluid.

5. Conclusions

In this study, we employed the advanced numerical shooting method to derive a solution for the intricate two-dimensional Darcy-Forchheimer tri-hybrid ferrofluid system. This investigation delves into the complexities of coupled heat and mass transfer, featuring the presence of motile microorganisms, over an unsteady, incompressible porous surface subjected to activation energy and chemical reactions. Rigorous evaluation, both mathematically and graphically, was conducted to ascertain the precision of the numerical shooting methodology in comparison to the numerical model, confirming its robust compatibility with empirical data. Subsequent to this validation, our exploration extended to scrutinizing the nuanced impacts of various advanced physical parameters, including Darcy porous medium (F), Reynolds number (Re), Prandtl number (Pr), Peclet number (Pe), thermal activation energy (α), and species volume friction coefficient parameters

$(\varphi_1, \varphi_2, \varphi_3)$, among others. These analyses shed light on the intricate relationships between these parameters and key flow variables such as velocity, temperature, concentration, and the significance of motile microorganisms. The results are visually presented, and the quantitative impact is concisely summarized in tabular form, elucidating parameters such as Skin Friction, Nusselt Number, Sherwood Number, and Motile Number. This study unequivocally concludes that:

- Augmented values of the Darcy porous medium (F) correspond to an intensified skin friction coefficient in both porous mediums.
- As the Peclet number (Pe) values increase, there is an enhancement in the flow of the Motile number on the lower porous surface, while a reduction is observed on the upper surface.
- Elevating the values of the porous medium parameter (r) leads to an enhancement in shear stress, thereby positively influencing both the thickness of the momentum boundary layer.
- Increasing the activation energy (E) parameter values results in a decline in the convective flux of heat and mass transfer.
- As the Schmidt number attains its highest values, denoted as (Sc or Sb), there is a gradual reduction observed in the flow of mass and motile microorganism transfer.
- The variables α and Re directly influence the components of shear stress and heat transfer, wherein an increase in α and Re corresponds to a reduction in both shear stress and heat transfer.
- The presence of positive values for both the Similarity Variable (n) and Exothermic/Endothermic parameter (λ) leads to an enhancement in the flow of thermal transfer on both porous surfaces.
- In comparison to Ferro and hybrid ferrofluid, the heat transfer rate is notably superior in ternary hybrid ferrofluid.
- An increase in the values of the magnetic parameter corresponds to an enhanced flow of momentum boundary layer thickness in the radial velocity profile for both porous surfaces.

Funding

This work was supported by the Fundamental Research Funds for the Central Universities (Grant No. D5000230061) and the authors extend their appreciation to the Deputyship for Research & Innovation, Ministry of Education in Saudi Arabia for funding this research work through the project number ISP23-66.

ORCID

Qadeer Raza  <http://orcid.org/0009-0008-4831-5606>

Ali J. Chamkha  <http://orcid.org/0000-0002-8335-3121>

References

- [1] E. A. Algehyne, Y. Y. Alhusayni, A. Tassaddiq, A. Saeed and M. Bilal, "The study of nanofluid flow with motile microorganisms and thermal slip condition across a vertical permeable surface," *Waves Rand. Comp. Med.*, vol. 6, pp. 1–18, 2022. DOI:10.1080/17455030.2022.2071501.
- [2] S. Maatoug, *et al.*, "Bioconvective Homann flow of tangent hyperbolic nanofluid due to spiraling disk with convective and zero mass flux constraints," *J. Indian Chem. Soc.*, vol. 100, no. 1, pp. 100819, 2023. DOI:10.1016/j.jics.2022.100819.
- [3] S. Ahmad, M. Ashraf and K. Ali, "Heat and mass transfer flow of gyrotactic microorganisms and nanoparticles through a porous medium," *IJHT*, vol. 38, no. 2, pp. 395–402, 2020. DOI:10.18280/ijht.380215.
- [4] V. Puneeth, M. I. Khan, S. S. Narayan, E. R. El-Zahar and K. Guedri, "The impact of the movement of the gyrotactic microorganisms on the heat and mass transfer characteristics of Casson nanofluid," *Waves Random Complex Media*, vol. 2, pp. 1–24, 2022. DOI:10.1080/17455030.2022.2055811.

- [5] H. A. Madkhali, A. Salmi, S. O. Alharbi and A. S. Alqahtani, "Impact of hybrid nanoparticles on heat and mass transfer in the presence of movement of motile gyrotactic microorganisms," *Waves Random Complex Media*, vol. 5, pp. 1–19, 2022. DOI:10.1080/17455030.2022.2140858.
- [6] M. Elayarani, M. Shanmugapriya and P. S. Kumar, "Intensification of heat and mass transfer process in MHD carreau nanofluid flow containing gyrotactic microorganisms," *Chem. Eng. Proces. Process Intensificat.*, vol. 160, no. 1, pp. 108299, 2021. DOI:10.1016/j.cep.2021.108299.
- [7] Z. Nisar and H. Yasmin, "Analysis of motile gyrotactic micro-organisms for the bioconvection peristaltic flow of carreau-yasuda bionanomaterials," *Coatings*, vol. 13, no. 2, pp. 314–2, 2023. DOI:10.3390/coatings13020314.
- [8] A. Al-Bossly, F. S. Alduais, S. A. Lone, M. Y. Almusawa and A. Saeed, "A stratified MHD flow of Eyring-Powell fluid containing gyrotactic microorganisms through a stretching sheet with mixed convection," *ZAMM-J. APPL Mathemat. Mechan. Zeitschr. Für Angewand. Mathem. Und Mechan.*, vol. 103, no. 9, pp. e202200492, 2023. DOI:10.1002/zamm.202200492.
- [9] M. Madhavi and P. Sravanthi, "Nanofluid flow in presence of gyrotactic microorganisms on the stretching surface with magnetic field and activation energy," *Front. Heat Mass Transfer (FHMT)*, vol. 30, no. 19, pp. 8, 2022. DOI:10.5098/hmt.19.40.
- [10] R. Pourrajab and A. Noghrehabadi, "Bioconvection of nanofluid past stretching sheet in a porous medium in presence of gyrotactic microorganisms with newtonian heating," *MATEC Web. Conf.*, vol. 220, pp. 01004, 2018. DOI:10.1051/mateconf/201822001004.
- [11] S. Ahmad, M. Ashraf and K. Ali, "Nanofluid flow comprising gyrotactic microorganisms through a porous medium," *J. App. Flu. Mech.*, vol. 13, no. 5, pp. 1539–49, 2020. DOI:10.36884/jafm.13.05.31030.
- [12] S. K. Mondal and D. Pal, "Computational analysis of bioconvective flow of nanofluid containing gyrotactic microorganisms over a nonlinear stretching sheet with variable viscosity using HAM," *J. Comp. Des. Eng.*, vol. 7, no. 2, pp. 251–267, 2020. DOI:10.1093/jcde/qwaa021.
- [13] N. S. Khashi'le, I. Waini, N. S. Wahid, N. M. Arifin and I. Pop, "Radiative hybrid ferrofluid flow over a permeable shrinking sheet in a three-dimensional system," *CFD Lett.*, vol. 14, no. 11, pp. 9–21, 2022. DOI:10.37934/cfdl.14.11.921.
- [14] W. M. Rosli, M. K. Mohamed, N. M. Sarif, N. F. Mohammad and S. K. Soid, "Blood conveying ferroparticle flow on a stagnation point over a stretching sheet: non-newtonian williamson hybrid ferrofluid," *J. Adv. Res. Flu. Mech. Ther. Sci.*, vol. 97, no. 2, pp. 175–85, 2022. DOI:10.37934/arfmts.97.2.175185.
- [15] K. Anantha Kumar, N. Sandeep, V. Sugunamma and I. L. Animasaun, "Effect of irregular heat source/sink on the radiative thin film flow of MHD hybrid ferrofluid," *J. Therm. Anal. Calorim.*, vol. 139, no. 3, pp. 2145–2153, 2022. DOI:10.1007/s10973-019-08628-4.
- [16] S. Zainodin, A. Jamaludin, R. Nazar and I. Pop, "MHD mixed convection of hybrid ferrofluid flow over an exponentially stretching/shrinking surface with heat source/sink and velocity slip," *Mathematics*, vol. 10, no. 23, pp. 4400–11, 2022. DOI:10.3390/math10234400.
- [17] S. Saranya, Q. M. Al-Mdallal and S. Javed, "Shifted legendre collocation method for the solution of unsteady viscous-ohmic dissipative hybrid ferrofluid flow over a cylinder," *Nanomaterials*, vol. 11, no. 6, pp. 1512, 62021. DOI:10.3390/nano11061512.
- [18] K. Hosseinzadeh, S. Roghani, A. Asadi, A. Mogharrebi and D. D. Ganji, "Investigation of micropolar hybrid ferrofluid flow over a vertical plate by considering various base fluid and nanoparticle shape factor," *HFF*, vol. 31, no. 1, pp. 402–417, 2020. DOI:10.1108/HFF-02-2020-0095.
- [19] M. Bilal, *et al.*, "Numerical analysis of an unsteady, electroviscous, ternary hybrid nanofluid flow with chemical reaction and activation energy across parallel plates," *Micromach*, vol. 13, no. 6, pp. 874–5, 2022. DOI:10.3390/mi13060874.
- [20] M. D. Shamshuddin, N. Akkurt, A. Saeed and P. Kumam, "Radiation mechanism on ternary hybrid nanofluid flow through rotating disk encountered by Hall currents: HAM solution," *Alex. Eng. J.*, vol. 65, pp. 543–559, 2023. DOI:10.1016/j.aej.2022.10.021.
- [21] F. Shahzad *et al.*, "Second-order convergence analysis for Hall effect and electromagnetic force on ternary nanofluid flowing via rotating disk," *Sci. Rep.*, vol. 12, no. 1, pp. 18769, 2022. DOI:10.1038/s41598-022-23561-7.
- [22] S. O. Salawu, E. I. Akinola and M. D. Shamshuddin, "Entropy generation and current density of tangent hyperbolic Cu-C2H6O2 and ZrO2-Cu/C2H6O2 hybridized electromagnetic nanofluid: a thermal power application," *S. Afr. J. Chem. Eng.*, vol. 46, pp. 1–11, 2023. DOI:10.1016/j.sajce.2023.07.003.
- [23] A. B. Patil, *et al.*, "MHD-driven chemically active and thermally radiative Prandtl hybrid nanofluid flow on stretching device with Ohmic heating, dissipation, and diffusion effects," *Numer Heat Tr A- Appl.*, pp. 1–18, 2023. DOI:10.1080/10407782.2023.2219832.
- [24] M. D. Shamshuddin, *et al.*, "Thermal examination of chemical interaction and thermophoretic diffusion of Williamson fluid flow across Riga Plate surface with nonlinearity radiation flux," *Numer Heat Tr A- Appl.*, pp. 1–15, 2023. DOI:10.1080/10407782.2023.2251092.

- [25] T., Islam, M., Ferdows, M. D., Shamshuddin, M. S., Alqarni, “Sisko fluid modeling and numerical convective heat transport analysis over-stretching device with radiation and heat dissipation,” *Numer Heat Tr A- Appl.*, pp. 1–19, 2023. DOI:10.1080/10407782.2023.2200046.
- [26] Q. Raza, X. Wang, F. Ullah Khan and A. J. Chamkha, “Role of Lorentz force and nanoparticles morphology on the dynamics of ternary hybrid nanofluid flow subject to porous disks and gyrotactic microorganisms,” *Numer Heat Tr A- Appl.*, pp. 1–24, 2023. DOI:10.1080/10407782.2023.2290084.
- [27] Q. Raza, et al., “Significance role of dual porosity and interfacial nanolayer mechanisms on hybrid nanofluids flow: a symmetry flow model,” *Mod. Phys. Lett. B*, vol. 38, no. 08, pp. 2450022, 2023. DOI:10.1142/S0217984924500222.
- [28] Q. Raza, et al., “Mathematical modeling of nanolayer on biological fluids flow through porous surfaces in the presence of CNT,” *Case Stud Therm Eng.*, vol. 45, pp. 102958–4, 2023. DOI:10.1016/j.csite.2023.102958.
- [29] Q. Raza, et al., “Insight into dynamic of mono and hybrid nanofluids subject to binary chemical reaction, activation energy, and magnetic field through the porous surfaces,” *Math*, vol. 10, no. 16pp., pp. 3013–8, 2022. DOI:10.3390/math10163013.
- [30] I. Tili, M. T. Mustafa, K. A. Kumar and N. Sandeep, “Effect of asymmetrical heat rise/fall on the film flow of magnetohydrodynamic hybrid ferrofluid,” *Sci. Rep.*, vol. 10, no. 1, pp. 6677, 2020. DOI:10.1038/s41598-020-63708-y.
- [31] N. S. Anuar, N. Bachok and I. Pop, “Influence of MHD hybrid ferrofluid flow on exponentially stretching/shrinking surface with heat source/sink under stagnation point region,” *Math*, vol. 9, no. 22, pp. 2932–11, 2021. vol. DOI:10.3390/math9222932.
- [32] N. Sandeep, S. P. Samrat and G. P. Ashwinkumar, “Flow and heat transfer in radiative MHD dusty-hybrid ferrofluids,” *Waves Rand. Comp. Med.*, vol. 18, pp. 1–14, 2022. DOI:10.1080/17455030.2022.2036866.
- [33] M. Ferdows and J. C. Misra, “Heat and mass transfer during MHD flow of a nanofluid containing gyrotactic microorganisms on a stretching/shrinking sheet,” *Multiscale Sci. Eng.*, vol. 4, no. 1–2, pp. 55–65, 2022. DOI:10.1007/s42493-022-00077-w.
- [34] M. D. Hossain, M. A. Samad and M. M. Alam, “Study of MHD heat and mass transfer flow for hall and ion-slip currents effects in high porosity medium and revolving system,” *AJAMS*, vol. 6, no. 67pp., pp. 100–125, 2020. DOI:10.32861/ajams.67.100.125.
- [35] A. J. Chamkha and S. E. Ahmed, “Unsteady MHD heat and mass transfer by mixed convection flow in the forward stagnation region of a rotating sphere at different wall conditions,” *Chem. Eng. Comm.*, vol. 199, no. 1, pp. 122–141, 2012. DOI:10.1080/00986445.2011.575907.
- [36] A. Rauf, N. A. Shah, A. Mushtaq and T. Botmart, “Heat transport and magnetohydrodynamic hybrid micropolar ferrofluid flow over a non-linearly stretching sheet,” *MATH*, vol. 8, no. 1, pp. 164–193, 2023. DOI:10.3934/math.2023008.
- [37] T. Muhammad, A. Alsaedi, S. A. Shehzad and T. Hayat, “A revised model for Darcy-Forchheimer flow of Maxwell nanofluid subject to convective boundary condition,” *Chin. J. Phy.*, vol. 55, no. 3, pp. 963–976, 2017. DOI:10.1016/j.cjph.2017.03.006.
- [38] M. Sheikholeslami and A. J. Zeeshan, “Numerical simulation of Fe₃O₄-water nanofluid flow in a non-Darcy porous media,” *HFF*, vol. 28, no. 3pp., pp. 641–660, 2018. DOI:10.1108/HFF-04-2017-0160.
- [39] R. S. Saif, T. Hayat, R. Ellahi, T. Muhammad and A. Alsaedi, “Darcy-Forchheimer flow of nanofluid due to a curved stretching surface,” *HFF*, vol. 29, no. 1, pp. 2–20, 2018. DOI:10.1108/HFF-08-2017-0301.
- [40] A. Majeed, A. Zeeshan and F. M. Noori, “Numerical study of Darcy-Forchheimer model with activation energy subject to chemically reactive species and momentum slip of order two,” *AIP Advan.*, vol. 9, no. 4, pp. 045035, 2019. DOI:10.1063/1.5095546.
- [41] R. J. PunithGowda, R. N. Kumar and B. C. Prasanna Kumara, “Two-phase Darcy-Forchheimer flow of dusty hybrid nanofluid with viscous dissipation over a cylinder,” *Inter. J. App. Compu. Math.*, vol. 7, no. 3, pp. 95–6, 2021. DOI:10.1007/s40819-021-01033-2.
- [42] H. B. Mallikarjuna, T. Nirmala, R. J. Punith Gowda, R. Manghat and R. S. Varun Kumar, “Two-dimensional Darcy-Forchheimer flow of a dusty hybrid nanofluid over a stretching sheet with viscous dissipation,” *Heat Trans.*, vol. 50, no. 4, pp. 3934–3947, 2021. DOI:10.1002/htj.22058.
- [43] A. Alshehri and Z. Shah, “Computational analysis of viscous dissipation and Darcy-Forchheimer porous medium on radioactive hybrid nanofluid,” *Case Stud. Therm. Eng.*, vol. 30, no. 1, pp. 101728–2, 2022. DOI:10.1016/j.csite.2021.101728.
- [44] S. Nasir, A. S. Berrouk, A. Tassaddiq, A. Aamir, N. Akkurt and T. Gul, “Impact of entropy analysis and radiation on transportation of MHD advance nanofluid in porous surface using Darcy-Forchheimer model,” *Chem. Phys. Lett.*, vol. 811, pp. 140221–1, 2023. DOI:10.1016/j.cplett.2022.140221.
- [45] M. E. Essam and E. M. Abedel-Aal, “Darcy-Forchheimer flow of a nanofluid over a porous plate with thermal radiation and brownian motion,” *J. Nanofluids*, vol. 12, no. 1, pp. 55–64, 2023. DOI:10.1166/jon.2023.1910.

- [46] R. Sindhu, N. Alessa, S. Eswaramoorthi and K. Loganathan, “Comparative analysis of darcy–forchheimer radiative flow of a water-based Al₂O₃-Ag/TiO₂ hybrid nanofluid over a riga plate with heat sink/source,” *Symmetry*, vol. 15, no. 1, pp. 199–1, 2023. DOI:10.3390/sym15010199.
- [47] H. Upreti, A. K. Pandey, M. Kumar and O. D. Makinde, “Darcy–Forchheimer flow of CNTs-H₂O nanofluid over a porous stretchable surface with Xue model,” *Int. J. Mod. Phys. B*, vol. 37, no. 02, pp. 2350018, 2023. DOI:10.1142/S0217979223500182.
- [48] M. P. Mkhathshwa and M. Khumalo, “Irreversibility scrutinization on EMHD Darcy–Forchheimer slip flow of Carreau hybrid nanofluid through a stretchable surface in porous medium with temperature-variant properties,” *Heat Trans.*, vol. 52, no. 1, pp. 395–429, 2023. DOI:10.1002/htj.22700.
- [49] S. Li, *et al.*, “Effects of activation energy and chemical reaction on unsteady MHD dissipative Darcy–Forchheimer squeezed flow of Casson fluid over horizontal channel,” *Sci. Rep.*, vol. 13, no. 1, pp. 2666, 2023. DOI:10.1038/s41598-023-29702-w.
- [50] W. Xiu, S. O. Salawu, O. Y. Oludoun, O. M. Ogunlaran and A. B. Disu, “Combined impact of Lorentz force, micro-rotation, and thermo-migration of particles: dynamics of micropolar fluids experiencing nonlinear thermal radiation and activation energy,” *J. Magn. Magn. Mater.*, vol. 569, pp. 170447, 2023. DOI:10.1016/j.jmmm.2023.170447.
- [51] A. Khan, *et al.*, “Bioconvection Maxwell nanofluid flow over a stretching cylinder influenced by chemically reactive activation energy surrounded by a permeable medium,” *Front. Phys.*, vol. 10, pp. 1348–1, 2023. DOI:10.3389/fphy.2022.1065264.
- [52] I. S. Hussain, D. Prakash, B. Abdalla and M. Muthamilselvan, “Analysis of Arrhenius activation energy and chemical reaction in nanofluid flow and heat transfer over a thin moving needle,” *CNANO*, vol. 19, no. 1, pp. 39–48, 2023. DOI:10.2174/1573413717666211117150656.
- [53] H. Dessie, “Effects of chemical reaction, activation energy and thermal energy on magnetohydrodynamics maxwell fluid flow in rotating frame,” *J. Nanofluids*, vol. 10, no. 1, pp. 67–74, 2021. DOI:10.1166/jon.2021.1767.
- [54] Z. Hussain and W. A. Khan, “Impact of thermal-solutal stratifications and activation energy aspects on time-dependent polymer nanoliquid,” *Waves Random Complex Media*, vol. 9, pp. 1–11, 2022. DOI:10.1080/17455030.2022.2128229.
- [55] M. Waqas, *et al.*, “Dynamics of bioconvective Casson nanoliquid from a moving surface capturing gyrotactic microorganisms, magnetohydrodynamics and stratifications,” *Therm. Sci. Eng. Prog.*, vol. 36, pp. 101492–12, 2022. DOI:10.1016/j.tsep.2022.101492.
- [56] M. Tabrez and W. Azeem Khan, “Exploring physical aspects of viscous dissipation and magnetic dipole for ferromagnetic polymer nanofluid flow,” *Waves Random Complex Media*, pp. 1–20, 102022. DOI:10.1080/17455030.2022.2135794.
- [57] N. Anjum, *et al.*, “Numerical analysis for thermal performance of modified Eyring Powell nanofluid flow subject to activation energy and bioconvection dynamic,” *Case Stud. Therm. Eng.*, vol. 39, pp. 102427–11, 2022. DOI:10.1016/j.csite.2022.102427.
- [58] M. Irfan, *et al.*, “Significance of non-Fourier heat flux on ferromagnetic Powell-Eyring fluid subject to cubic autocatalysis kind of chemical reaction,” *Int. Commun. Heatmass Transf.*, vol. 138, pp. 106374–11, 2022. DOI:10.1016/j.icheatmasstransfer.2022.106374.
- [59] W. A. Khan, “Significance of magnetized Williamson nanofluid flow for ferromagnetic nanoparticles,” *Waves Random Complex Media*, pp. 1–20, 2023. DOI:10.1080/17455030.2023.2207390.
- [60] W. A. Khan, “Impact of time-dependent heat and mass transfer phenomenon for magnetized Sutterby nanofluid flow,” *Waves Random Complex Media*, pp. 1–15, 2022. DOI:10.1080/17455030.2022.2140857.
- [61] W. A. Khan, Z. Arshad, A. Hobiny, S. Saleem, A. Al-Zubaidi and M. Irfan, “Impact of magnetized radiative flow of sutterby nanofluid subjected to convectively heated wedge,” *Int. J. Mod. Phys. B*, vol. 36, no. 16, pp. 2250079–5, 2022. DOI:10.1142/S0217979222500795.
- [62] W. A. Khan, M. Ali, M. Shahzad, F. Sultan, M. Irfan and Z. Asghar, “A note on activation energy and magnetic dipole aspects for Cross nanofluid subjected to cylindrical surface,” *Appl. Nanosci.*, vol. 10, no. 8, pp. 3235–3244, 2020. DOI:10.1007/s13204-019-01220-0.
- [63] W. A. Khan, M. Waqas, W. Chammam, Z. Asghar, U. A. Nisar and S. Z. Abbas, “Evaluating the characteristics of magnetic dipole for shear-thinning Williamson nanofluid with thermal radiation,” *Comput Methods Programs Biomed.*, vol. 191, pp. 105396, 2020. DOI:10.1016/j.cmpb.2020.105396.
- [64] W. A. Khan, “Dynamics of gyrotactic microorganisms for modified Eyring Powell nanofluid flow with bioconvection and nonlinear radiation aspects,” *Waves Random Complex Media*, pp. 1–11, 2023. DOI:10.1080/17455030.2023.2168086.
- [65] W. A. Khan, *et al.*, “Impact of nanoparticles and radiation phenomenon on viscoelastic fluid,” *Int. J. Mod. Phys. B*, vol. 36, no. 05, pp. 2250049, 2022. DOI:10.1142/S0217979222500497.

- [66] W. A. Khan, N. Anjum, M. Waqas, S. Z. Abbas, M. Irfan and T. Muhammad, "Impact of stratification phenomena on a nonlinear radiative flow of sutterby nanofluid," *J. Mater.*, vol. 15, pp. 306–314, 2021. DOI: [10.1016/j.jmrt.2021.08.011](https://doi.org/10.1016/j.jmrt.2021.08.011).
- [67] W. A. Khan, H. Sun, M. Shahzad, M. Ali, F. Sultan and M. Irfan, "Importance of heat generation in chemically reactive flow subjected to convectively heated surface," *Indian J. Phys.*, vol. 95, no. 1, pp. 89–97, 2021. DOI: [10.1007/s12648-019-01678-2](https://doi.org/10.1007/s12648-019-01678-2).
- [68] W. A. Khan, M. Ali, M. Irfan, M. Khan, M. Shahzad and F. Sultan, "A rheological analysis of nanofluid subjected to melting heat transport characteristics," *Appl. Nanosci.*, vol. 10, no. 8, pp. 3161–3170, 2020. DOI: [10.1007/s13204-019-01067-5](https://doi.org/10.1007/s13204-019-01067-5).
- [69] W. A. Khan, M. Waqas, S. Kadry, Z. Asghar, S. Z. Abbas and M. Irfan, "On the evaluation of stratification based entropy optimized hydromagnetic flow featuring dissipation aspect and Robin conditions," *Comput. Methods Programs Biomed.*, vol. 190, pp. 105347, 2020. DOI: [10.1016/j.cmpb.2020.105347](https://doi.org/10.1016/j.cmpb.2020.105347).
- [70] J. Majdalani, C. Zhou and C. A. Dawson, "The two-dimensional viscous flow between slowly expanding or contracting walls with weak permeability," *J. Biomech.*, vol. 35, no. 10, pp. 1399–1403, 10. 2002. DOI: [10.1016/S0021-9290\(02\)00186-0](https://doi.org/10.1016/S0021-9290(02)00186-0).
- [71] M. Z. Qureshi, *et al.*, "Activation energy performance through magnetized hybrid Fe₃O₄-PP nanofluids flow with impact of the cluster interfacial nanolayer," *Mathematics*, vol. 10, no. 18, pp. 3277, 2022. DOI: [10.3390/math10183277](https://doi.org/10.3390/math10183277).